Supporting Information

Deciphering the Aqueous Chemistry of Glyoxal Oxidation with Hydrogen Peroxide Using Molecular Imaging

Xiao Sui,[a, b] Yufan Zhou,[c,‡] Fei Zhang,[b,d,‡] Jianmin Chen,[a,d,]* Zihua Zhu,[c,]* and Xiao-Ying Yu[b,]*

[a]Environment Research Institute, Shandong University, Jinan, 250100, China.
[b]Earth and Biological Sciences Directorate, Pacific Northwest National Laboratory, Richland, WA 99354, USA.
[c]Environmental and Molecular Science Laboratory, Pacific Northwest National Laboratory, Richland, WA 99354, USA.
[d]Shanghai Key Laboratory of Atmospheric Particle Pollution and Prevention, Fudan Tyndall Centre, Department of Environmental Science & Engineering, Fudan University, Shanghai 200433, China
[≠]Equal contribution

*Corresponding authors: Xiao-Ying Yu:xiaoying.yu@pnnl.gov;1-509-372-4524;

Jianmin Chen: jmchen@sdu.edu.cn; 86-021-6564-2298; Zihua Zhu: zihua.zhu@pnnl.gov; phone 1-509-371-6240.

Experimental Details

Liquid sample preparation

A summary of the samples studied in this work is listed in the supplemental Table S1. Namely, various controls including UV, glyoxal, H_2O_2, and deionized (DI) water were analyzed. Glyoxal (Fisher scientific, 40% wt. solution in water, electrophoresis grade), hydrogen peroxide (H_2O_2), (Fisher scientific, 30% wt. solution in water, certified ACS) and DI water (18.2 MΩ) dispensed from a Barnstead water purification system (Model: Nanopure diamond) were used. Before an experiment, the pH of each solution was determined using a pH meter (ORION pH meter, 410A). Figure S2 shows the experimental photochemical aging setup of aqueous samples inside the microfluidic channel. The sample concentrations were similar to an early work by Carlton et al. concerning atmospheric relevance and for ease of result comparisons.[1]

Dry sample preparation

Prior to sample preparation, the Si wafer was pretreated with acetone, isopropanol, and high-purity DI water for 1 min each. After thorough cleaning, UV-Ozone plasma was used to get rid of residual organic contaminations on the Si wafer surface for 1-2 min. Sample preparation was done in the fume hood. About 20 μL reference acid (1mg/ml oxalic acid, malonic acid, succinic acid, malic acid and tartaric acid, respectively) solution was deposited on the clean Si wafer surface. The Si wafer was covered by the petri dish and put in the hood to dry. Then the dry sample was analyzed by ToF-SIMS immediately.

Additional experimental results including figures and tables are provided below. The following figures and tables are provided to substantiate the results and discussion section.
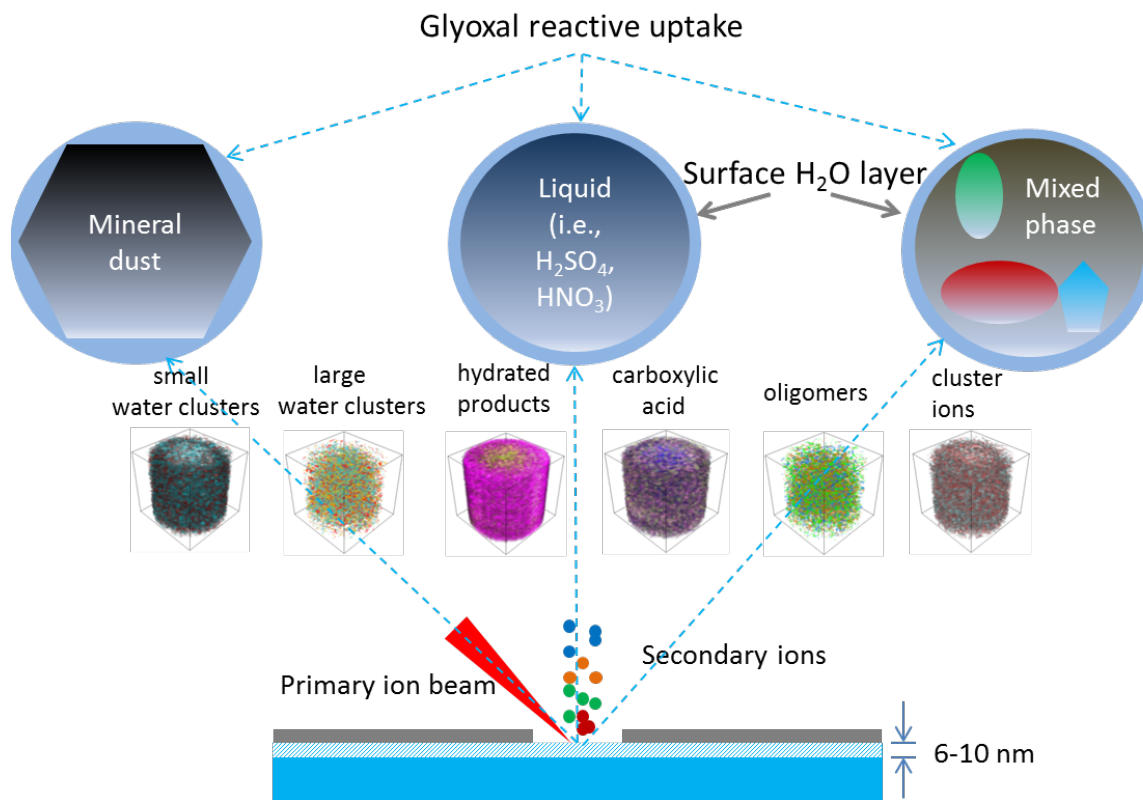
Supplementary Figures

Figure S1. Schematic of glyoxal reactive uptake on atmospheric aerosol aqueous surfaces simulated by using the SALVI and liquid ToF-SIMS approach employed in this study.

In the atmosphere, glyoxal uptake on different types of atmospheric aerosol aqueous surface layers can be followed using the in situ SALVI and liquid ToF-SIMS (a.k.a., liquid-vacuum interface) approach to approximate the liquid-air interface. There is a surface water layer (several nanometer thick) exist on the aerosol (adsorbed water or deliquesced) surface,[6] the thickness is consistent with the depth of liquid-SIMS detection (about 6-10 nm).
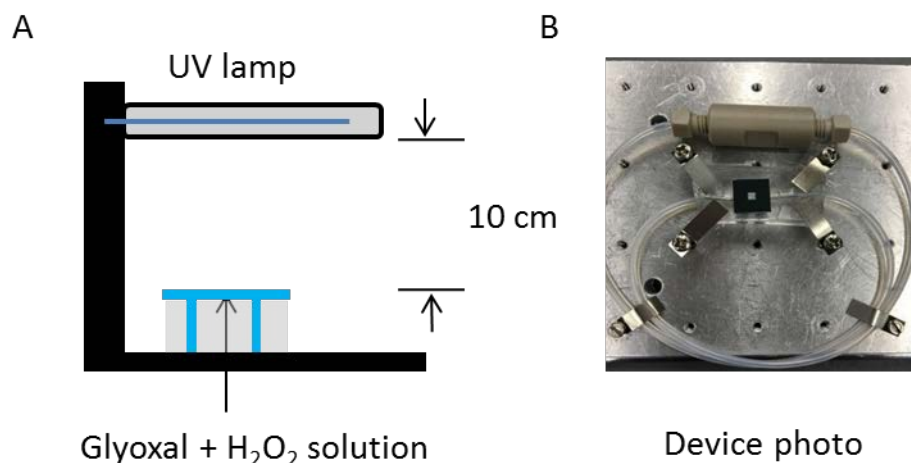
Figure S2. (a) Schematic of the photochemical aging setup and **(b)** a photo of a SALVI device assembled on the SIMS stage prior to liquid SIMS analysis.

An Hg-Ar UV lamp (ORIEL instruments, model 6060 spectral lamp) was used as the UV source. The distance between the SiN membrane and the UV lamp was 10 cm for all samples. When preparing for a photochemical reaction, glyoxal and hydrogen peroxide solution were mixed well before getting injected into the microchannel and put under the UV lamp immediately. The photochemical aging time reflected how long the sample was exposed under the UV lamp. Half an hour dark reaction time in the load lock was indispensable for each of the photochemical aging sample, because it took ~30 minutes to pump down to reach desirable vacuum in the SIMS chamber. When preparing for a dark reaction sample, the solution mixed time was considered to include two sections (outside the SIMS instrument and in the load lock). Thus, the device was wrapped with aluminum foil completely and set in an undisturbed area for controlled periods of time. Figure S2b depicts a SALVI device assembly on a SIMS stage after either UV aging or dark aging treatment, and it is ready for liquid SIMS analysis.
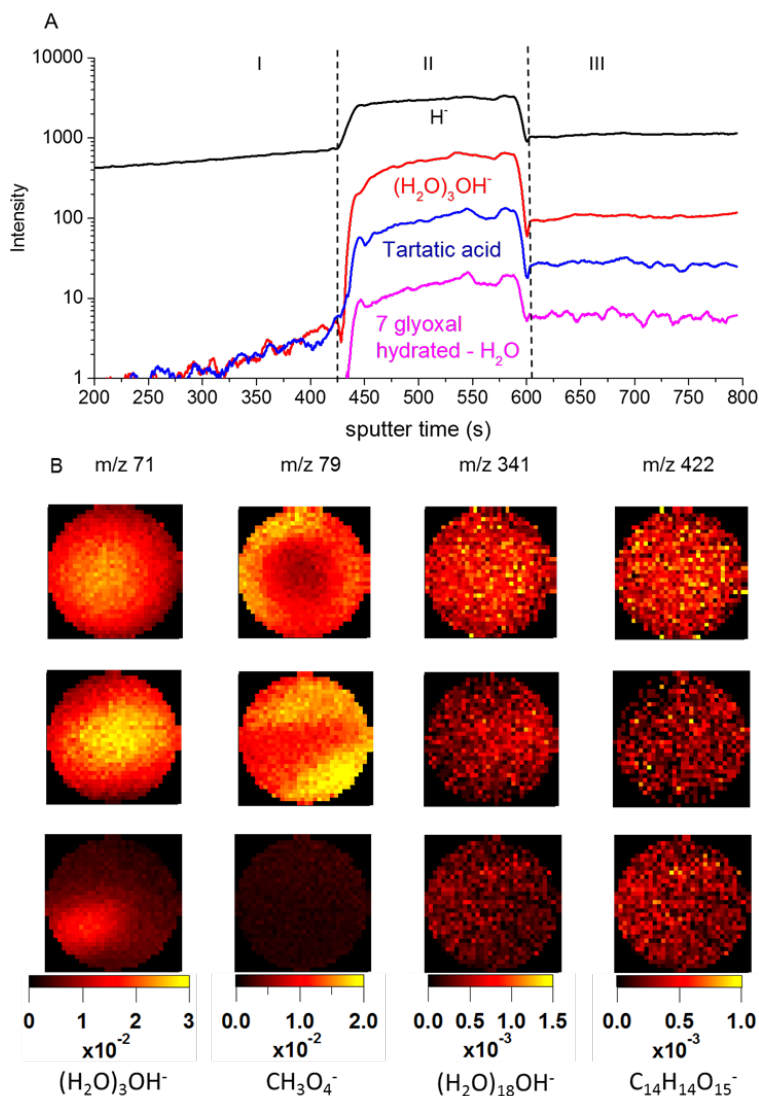
Figure S3. ToF-SIMS dynamic depth profiles of the 4 hr. UV aging sample in the negative mode. (A) Depth profile: Region I: before SiN membrane punch-through; Region II: imaging with wider pulse width for image reconstructions; Region III: imaging with a narrower pulse for mass spectrum reconstruction in the positive mode. (B) 2D image comparisons of key species under different experimental conditions (normalized to total ions).

Dynamic depth profiling

An example of SIMS dynamic depth profiling (positive mode) of a 4 hr. UV aging sample consisting initially of glyoxal and H_2O_2 was depicted in Figure 3. Negative depth profiling was also shown in Figure S3. Three regions existed along the depth profile time series. Region I corresponded to before the SiN membrane was punched through. Region II in the depth profile (Figure 3a) was constructed for 2D and 3D image comparison to study the distribution of different products in glyoxal and H_2O_2 aqueous surface reactions. The 2D image of water clusters showed different characteristics among photochemical reaction, dark reaction, and control samples. The photochemical reaction sample had lower counts of small water cluster than the dark reaction and control samples in the positive mode. However, higher counts of large water clusters in photochemical reaction samples were observed than the other two scenarios. In the negative mode, both small and large water cluster counts were higher in photochemical samples. In the

photochemical reaction sample, malonic acid (m/z$^+$ 105) had higher counts than those in photochemical reactions, indicating that it was one of the main products herein. The intensity of oligomer fragment peaks was higher in the UV treated sample, suggesting that oligomers were more likely to form under photochemical aging conditions compared to oxidation occurred in dark conditions.

In the positive depth profiling, peaks indicative of water (i.e., H$^+$, (H$_2$O)$_3$H$^+$, m/z$^+$ 55) had sharp increase at around 350 s, indicative of the SiN punch-through and observation of water in the positive mode (Figure S3a). Similarly, the peak intensity of water related peaks (i.e., H$^-$, (H$_2$O)$_3$OH$^-$), m/z$^-$ 71) increased at around 420 s in the negative mode (Figure S3a).[5, 7, 8] In Region II, the intensity of representative ions of oxidation products, such as tartaric acid (m/z$^-$ 149) and oligomers (C$_{14}$H$_{14}$O$_{15}$$^-$, m/z$^-$ 422) in the negative mode, had much higher intensity than Region I, indicating observations of the reaction products at the liquid surface. Region II lasted about 150 s to collect data with higher intensity and spatial resolution for image reconstructions. Then a narrower pulse was used for collecting data with relatively higher mass resolution in Region III. When the ion beam pulse width decreased, the intensity of chemical compounds also went down. Four peaks relevant to glyoxal oxidation products were chosen to show representative 2D images in the positive mode (Figure S3c), including a small water cluster ((H$_2$O)$_3$H$^+$, m/z$^+$ 55), malonic (m/z$^+$ 105), larger water cluster ((H$_2$O)$_{22}$H$^+$, m/z$^+$ 397) and oligomer (m/z$^+$ 327). In the negative mode, four peaks were selected including a small water cluster (i.e., (H$_2$O)$_3$OH$^-$, m/z$^-$ 71, H$_2$O…HCO$_3$ anion, m/z$^-$ 79), larger water cluster (i.e., (H$_2$O)$_{18}$OH$^-$, m/z$^-$ 341) and a representative oligomer (i.e. m/z$^-$ 422).
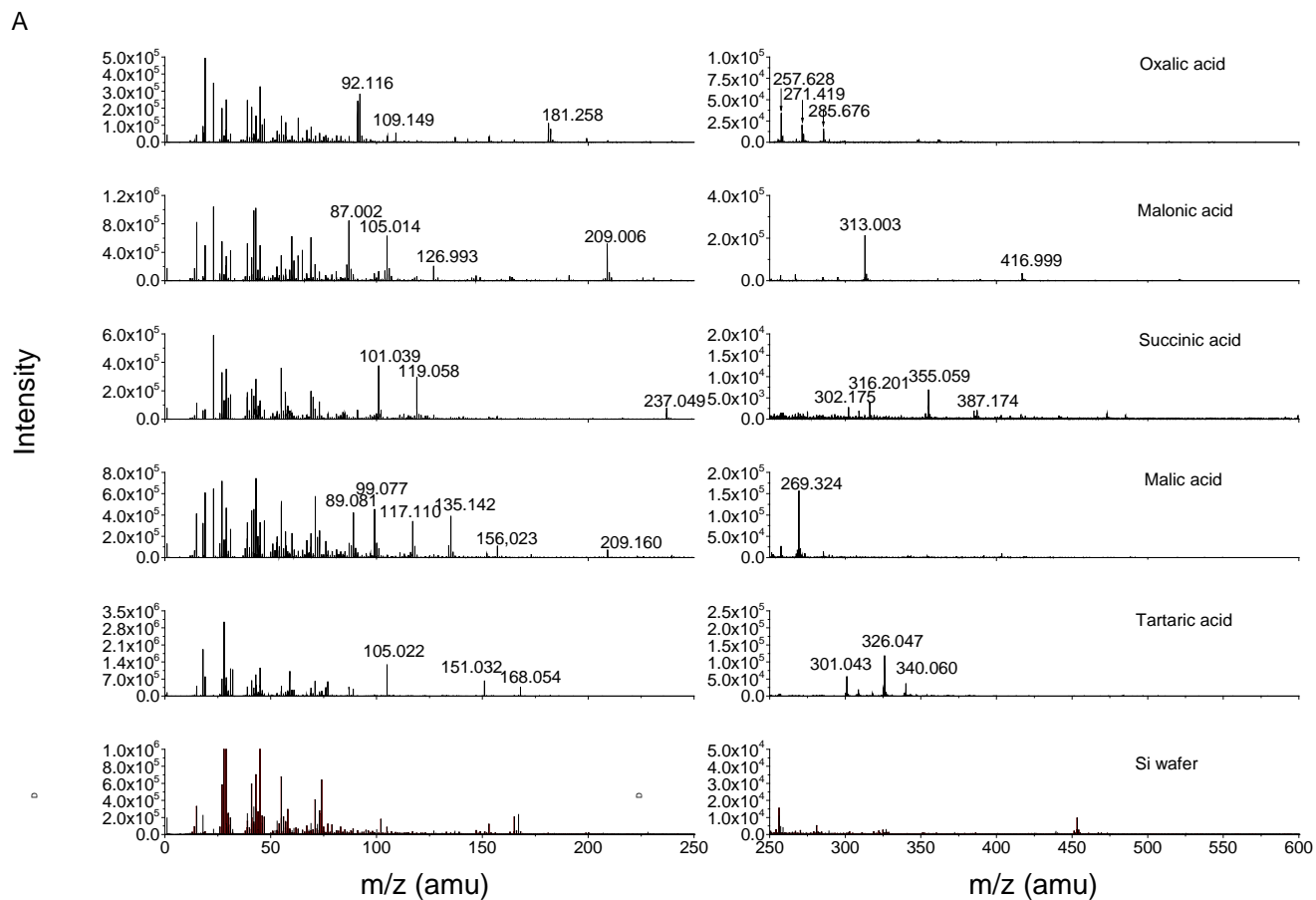
A

Figure S4a. Six dry reference samples (oxalic acid, malonic acid, succinic acid, malic acid, tartaric acid and Si wafer control) SIMS m/z spectral data (m/z 1-600) in the positive mode.

High mass resolution analysis using five dry reference samples was done to ascertain peak identifications in liquid-SIMS spectra. Dry sample preparation was detailed in SI. Several key products were observed in both dry and liquid samples (shown in Table S2). The mass to charge ratios (m/z) in dry and liquid SIMS were in good agreement, suggesting the unit mass identification in liquid SIMS was reliable.
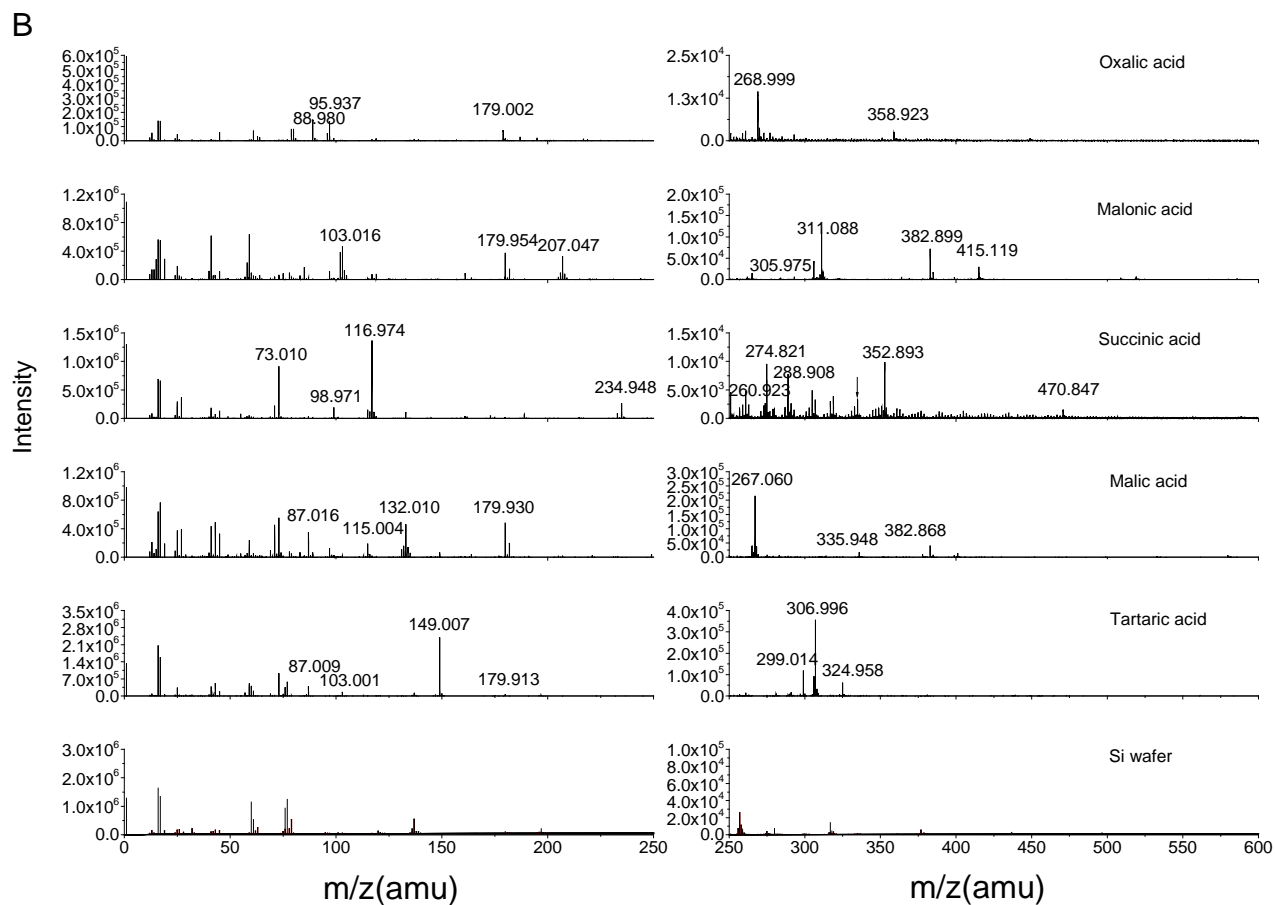
6

Figure S4b. Six dry reference samples (oxalic acid, malonic acid, succinic acid, malic acid, tartaric acid and Si wafer control) SIMS m/z spectral data (m/z 1-600) in the negative mode.

Similarly to Figure S4a, the negative spectral comparison was shown in Figure S4b negative spectra results also suggest the unit mass identification in liquid SIMS was reliable.
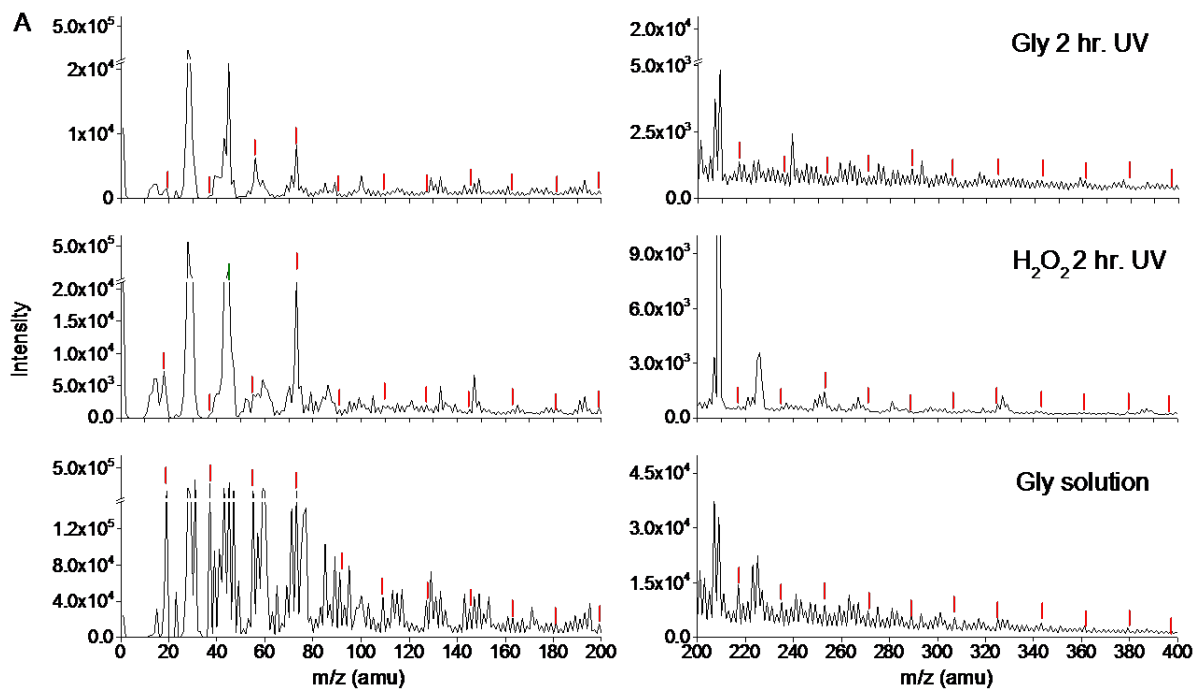
Figure S5a. Control samples raw spectra data m/z (1-400) in the positive mode. Red bars indicate locations of water clusters.

Three liquid control samples were also conducted. Their spectra were shown in Figure S5 to exclude uncertain factor of solution and instrument.
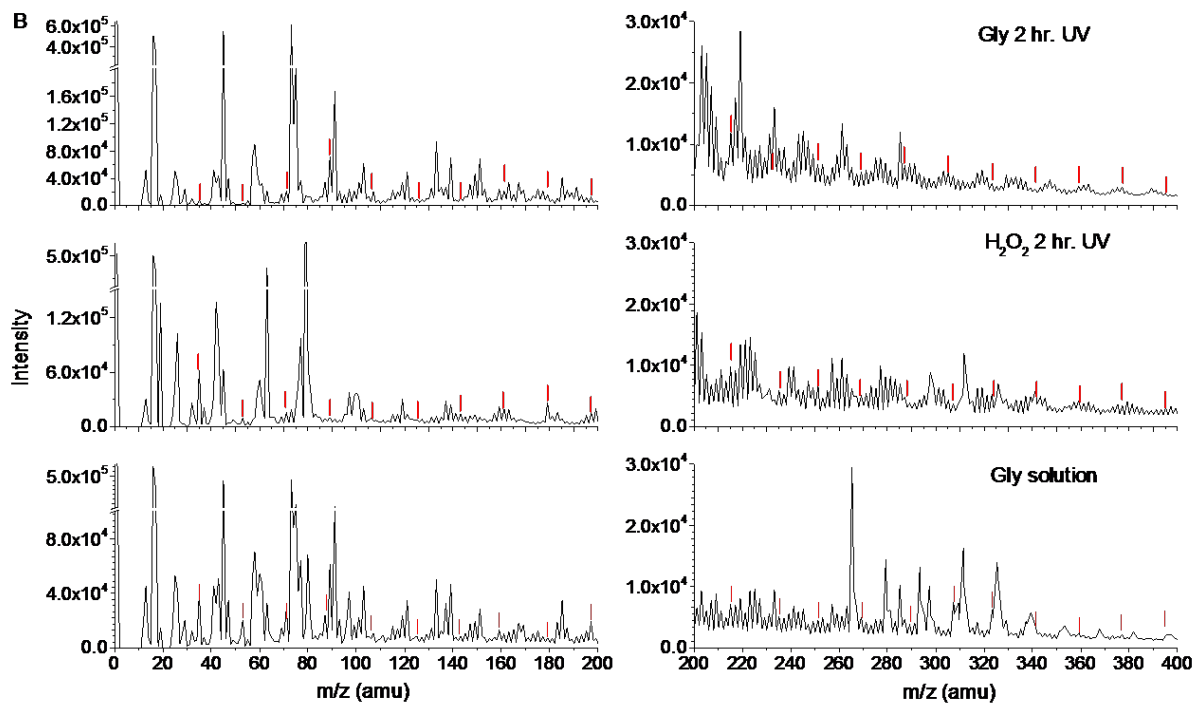
Figure S5b. Raw SIMS spectra of the control samples (m/z 1-400) in the negative ion mode. Red bars indicate locations of water clusters.

Comparison of UV, dark aging and control samples were conducted in Figure S6a to support the product identification in main text.
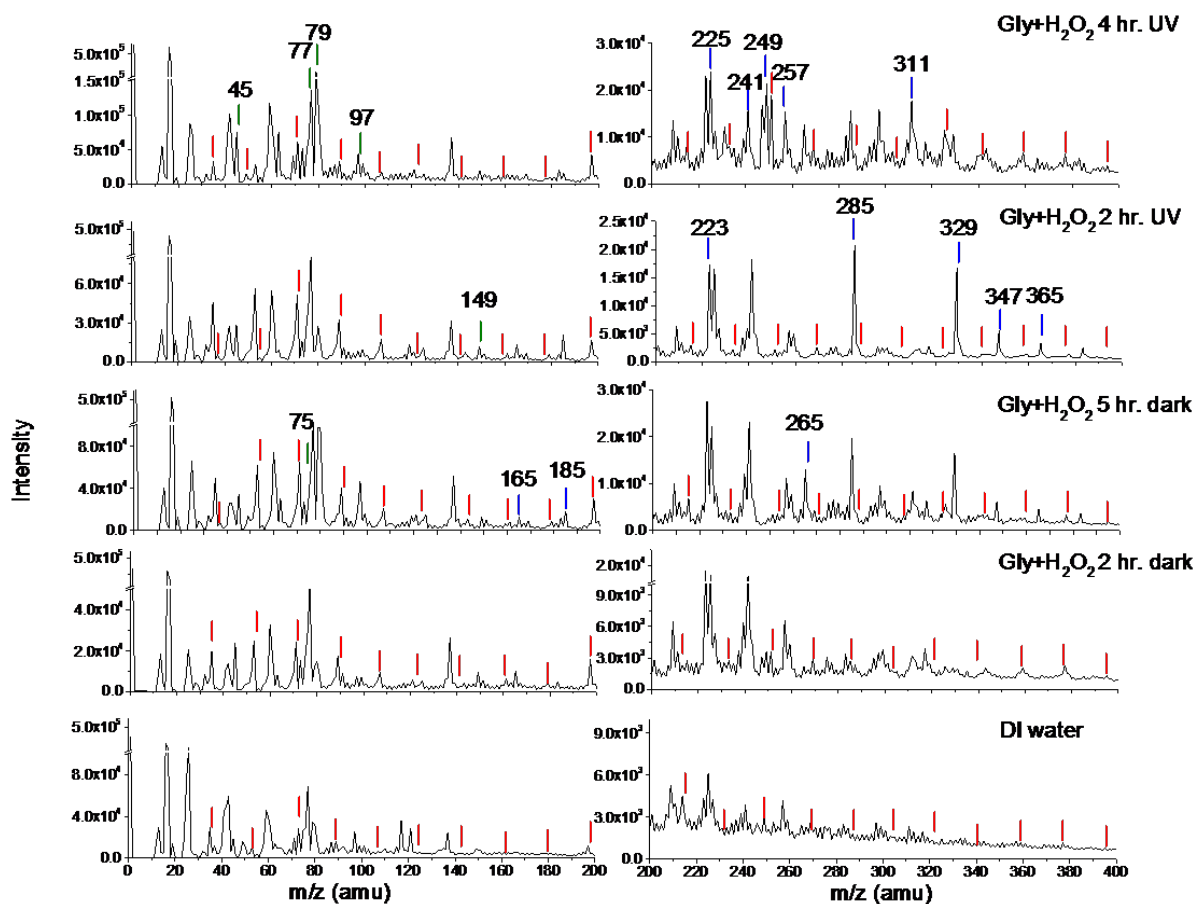
Figure S6. Raw SIMS spectra of the control samples (m/z 1-400) in the negative ion mode. Red bars indicate the location of water cluster peaks, green oxidation products, and blue polymer fragments.

Comparison of UV, dark aging and control samples in the negative were conducted in Figure S6 to support the product identification, in Figure 4 (in the positive mode), that different oxidation products, oligomers and cluster ions were formed under different photochemical conditions.

Figure S7a. ToF-SIMS spectral comparison of UV aging, dark reactions, and control samples in the positive ion mode (m/z 401-800). Red bars indicate locations of water clusters.

SIMS m/z spectra in the positive mode were shown in Figures S7a and S7b. Based on Figures S5a, S7a and S7b, interference peaks in the positive mode were excluded before peak identification and spectral PCA analysis, including H^+ (m/z=1), C^+ (m/z=12), CH^+ (m/z=13), CH_2^+ (m/z=14), CH_3^+ (m/z=15), $C_2H_3^+$ (m/z=27), Si^+ (m/z=28), $C_2H_5^+$ (m/z=29), $SiH2^+$ (m/z=30), $C_3H_5^+$(m/z=41), $SiHO^+$(m/z=45), $SiC3H9^+$ (m/z=73), $Si_2C_4H_{13}O^+$ (m/z=133), $Si_2C_5H_{15}O^+$(m/z=147), $Si_3C_5H_{15}O_3^+$ (m/z=207), Bi^+ (m/z=209), $C_{13}N_3H_{13}^+$(m/z=211), $C_{13}N_3H_{14}^+$(m/z=212), $C_{13}N_3H_{15}^+$(m/z=213), Bi_2^+(m/z=418) and Bi_3^+(m/z=627).

The comparison of UV, dark, and control samples ensures the formation of oxidation products. Oxidation products and oligomers were observed. Another observation was large water clusters, particularly in glyoxal + H_2O_2 5 hr. dark reaction samples. Here red markers show the location of water clusters, green markers show oxidation and hydration products and blue markers show polymer fragments.
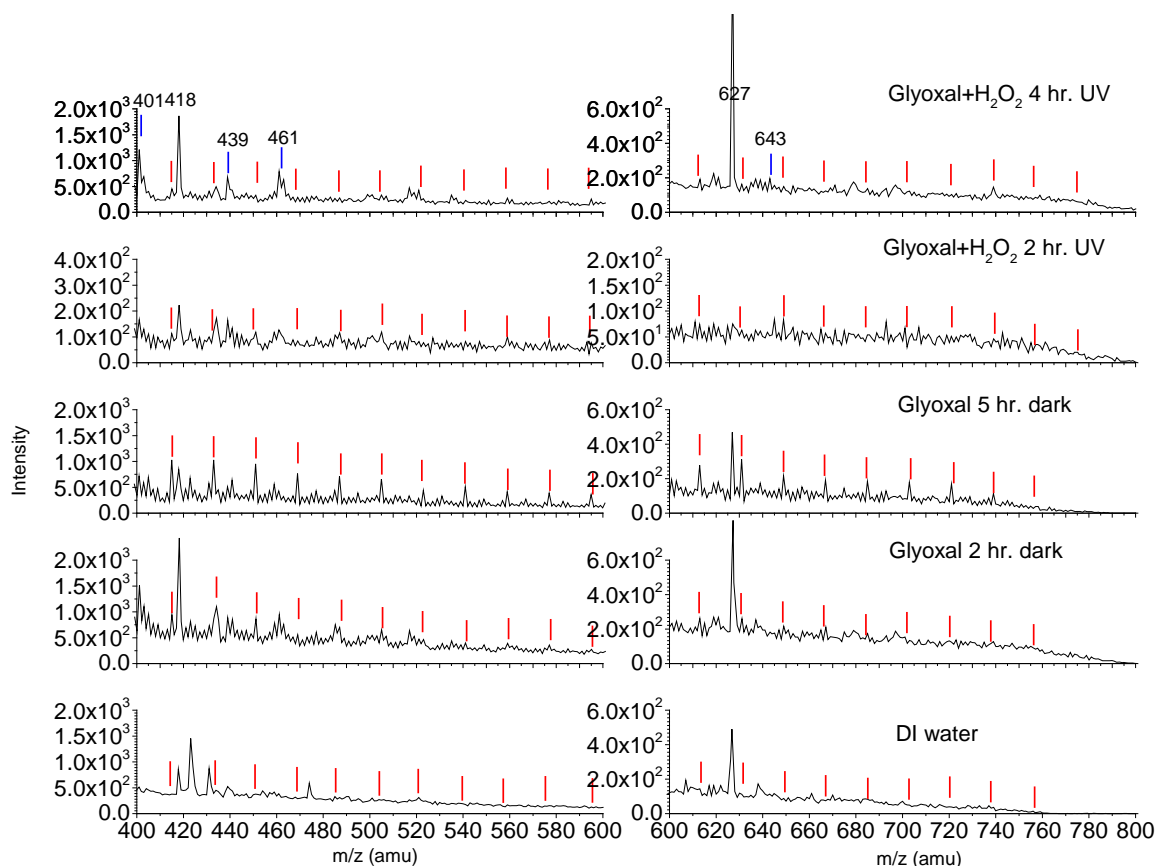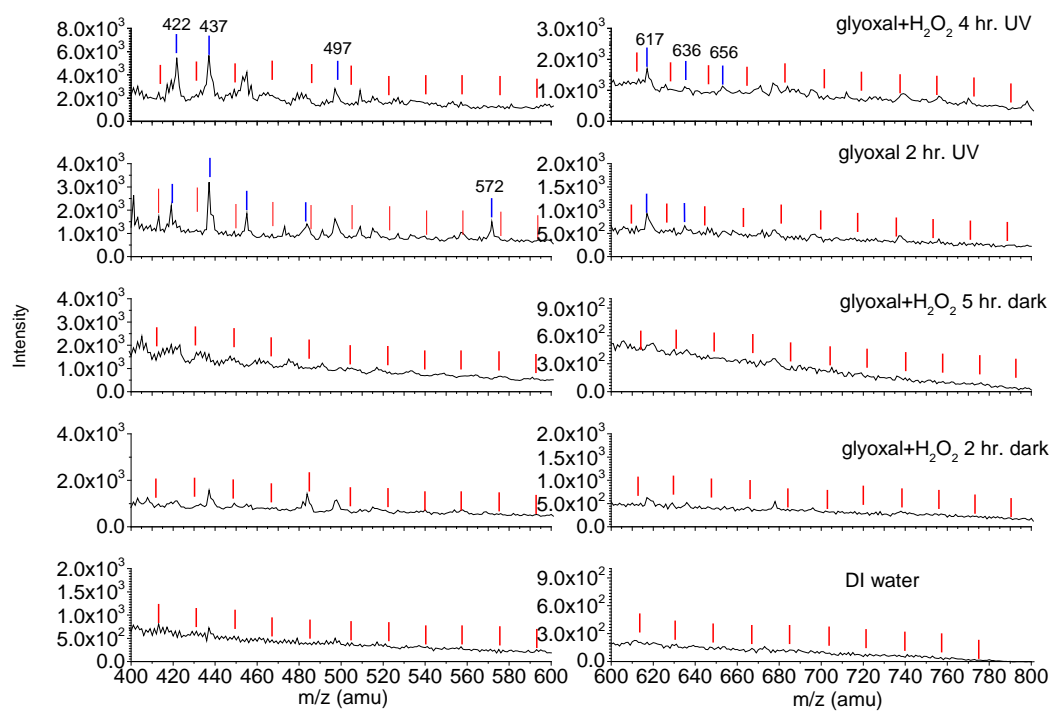
Figure S7b. ToF-SIMS spectral comparison of UV aging, dark reactions, and control samples in the negative ion mode (m/z 401-800). Red bars indicate locations of water clusters.
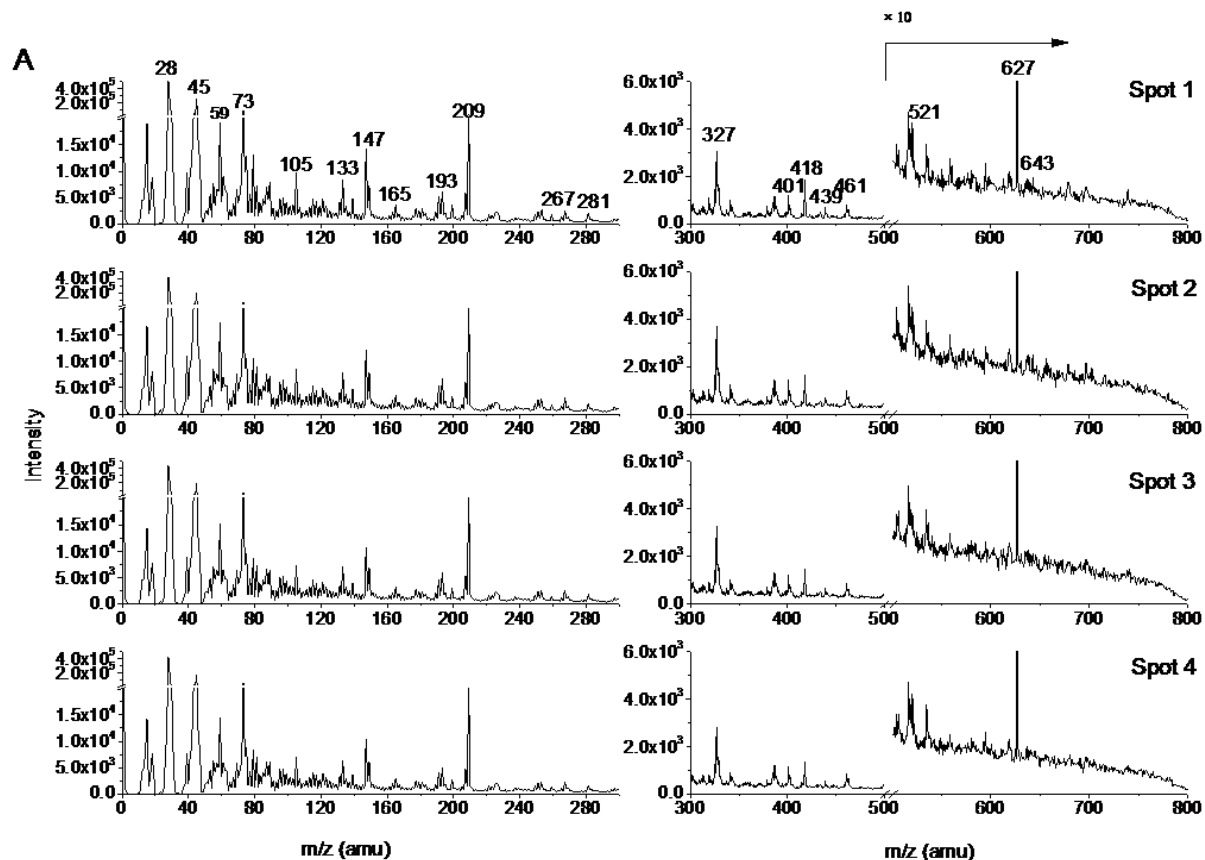
Figure S8a. Comparison of SIMS spectra of four different punch-through locations of the 4 hr. UV aging sample of glyoxal and H_2O_2 in the positive mode.

In order to evaluate spectral data quality, four different punch-through locations of glyoxal and H_2O_2 after 4 hours UV aging in the positive mode were depicted in Figure S8a. The spectra showed similar peak distribution and characteristics, indicating that that the reproducibility of liquid SIMS analysis was reliable.
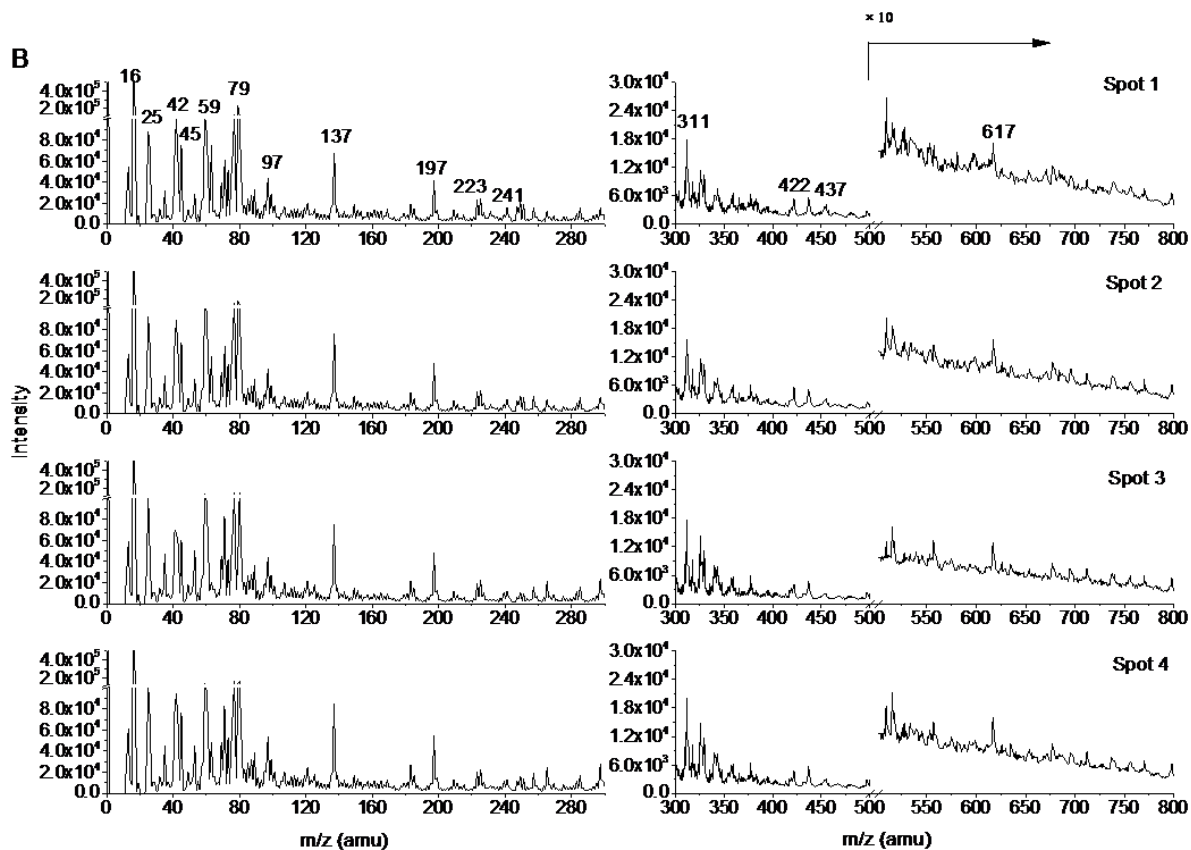
Figure S8b. Comparison of SIMS spectra of four different punch-through locations of the 4 hr. UV aging sample of glyoxal and H_2O_2 in the negative mode.

Different punch-through locations of Glyoxal and H_2O_2 4 hr. UV sample (4 negative plots) were depicted in Figure S8b. The figure demonstrated a similar distribution of most peaks, indicating that the analysis had good reproducibility.
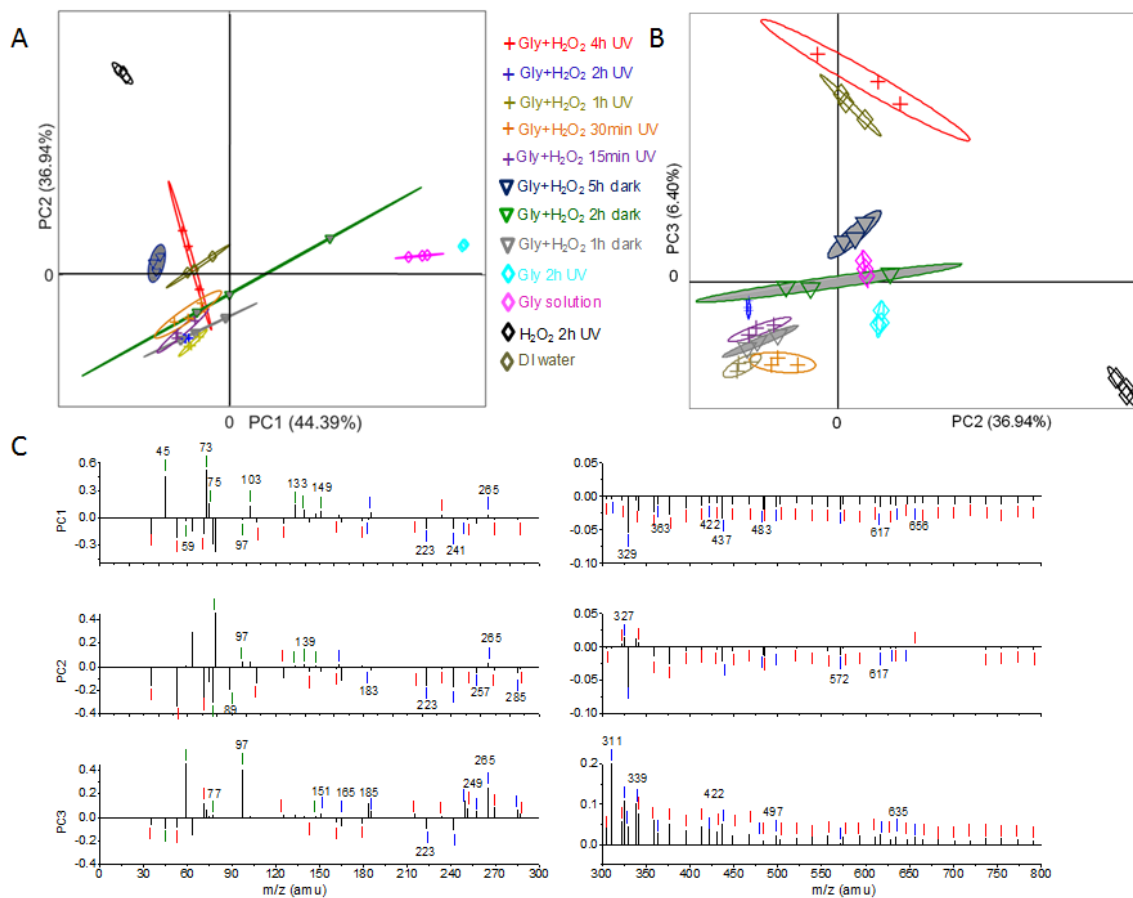
Figure S9. Spectral PCA analysis (normalized to selected peak total ions) in the negative mode: (A) PC1 vs. PC2 score plot, (B) PC2 vs. PC3 score plot, and (C) Loading plots of PC1, PC2 and PC3.

The negative spectral PCA score and loading plots were shown in Figure S9 to elucidate the key components among SIMS m/z spectra.
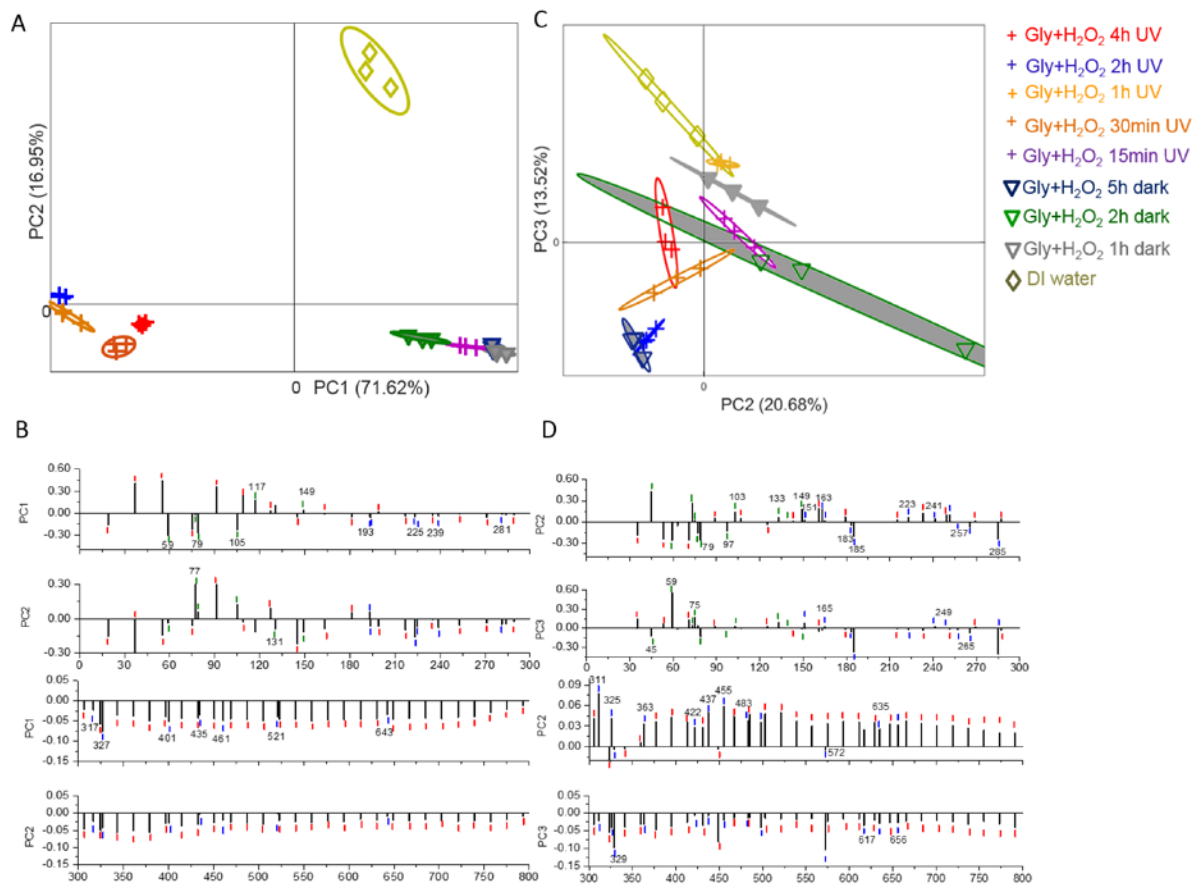
Figure S10. Spectral PCA analysis (normalized to selected peak total ions, control samples are excluded). (A) Score plot in the positive mode. (B) Loading plots in the positive mode. (C) Score plot negative mode. (D) Loading plot negative mode.

The plots are similar to the PCA results included all control samples. In the positive ion mode, short-time UV (15min) sample share common PC score with dark aging samples. Water clusters and various oxidation products and oligomers were main contributors of this separation to PCA loading. The peaks contributing to positive PC1 were mainly small water clusters, In contrast, larger water contribute to negative PC1. While in negative mode, because similar oxidation products are formed in both UV and dark samples, if control samples are excluded, different compounds cannot be clear identified. However, it is also suggest that short-time dark reactions share common features with 15 min-UV sample in the positive PC2 and PC3 loadings. Also, long-time aging on both dark and UV reactions favor the formation of large water clusters and oligomers in negative mode.
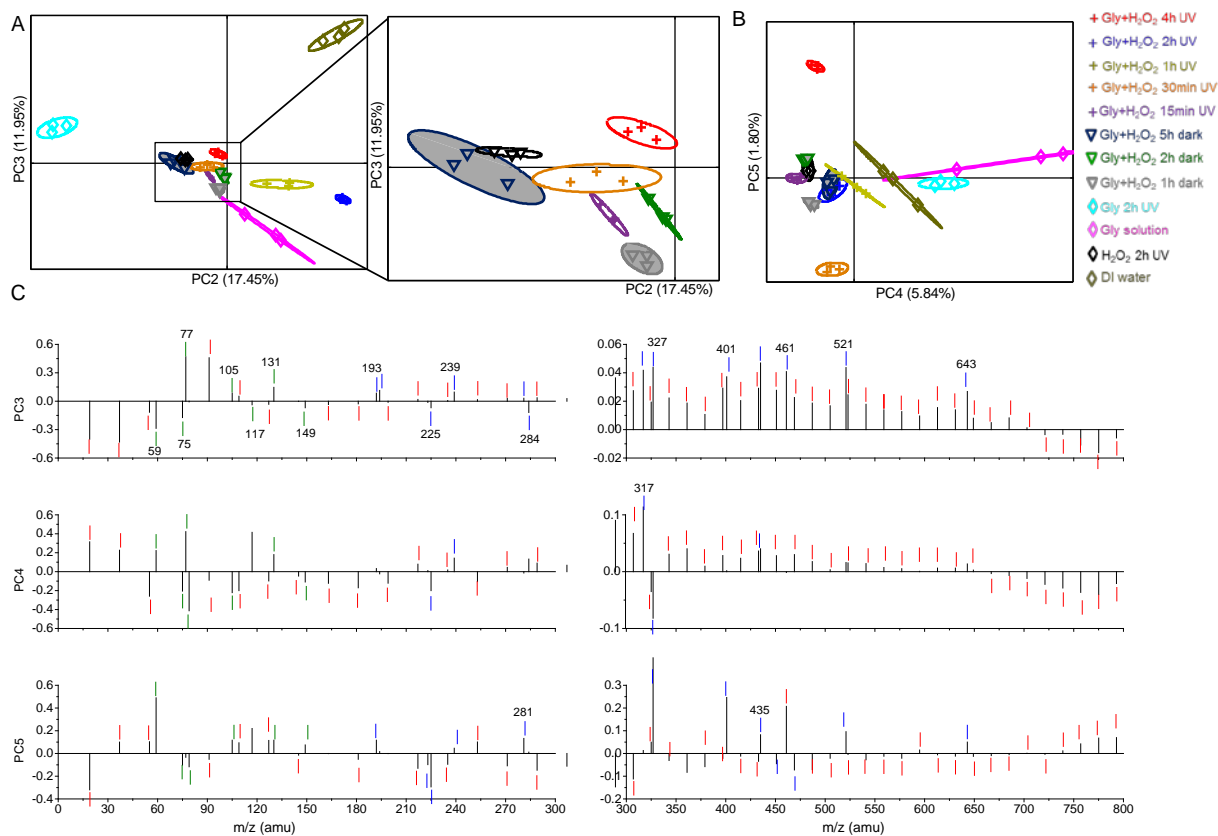
Figure S11. Selected peak spectral PCA analysis (normalized to the selected total ions) in the positive mode.(A) Score plot of PC2 vs. PC3. (B) Score plot of PC4 vs. PC5. (C) Loading plots of PC3, PC4 and PC5.

In the positive mode, other select peak PCA results were shown in Figure S11to support the results in Figure 4 in the main text.
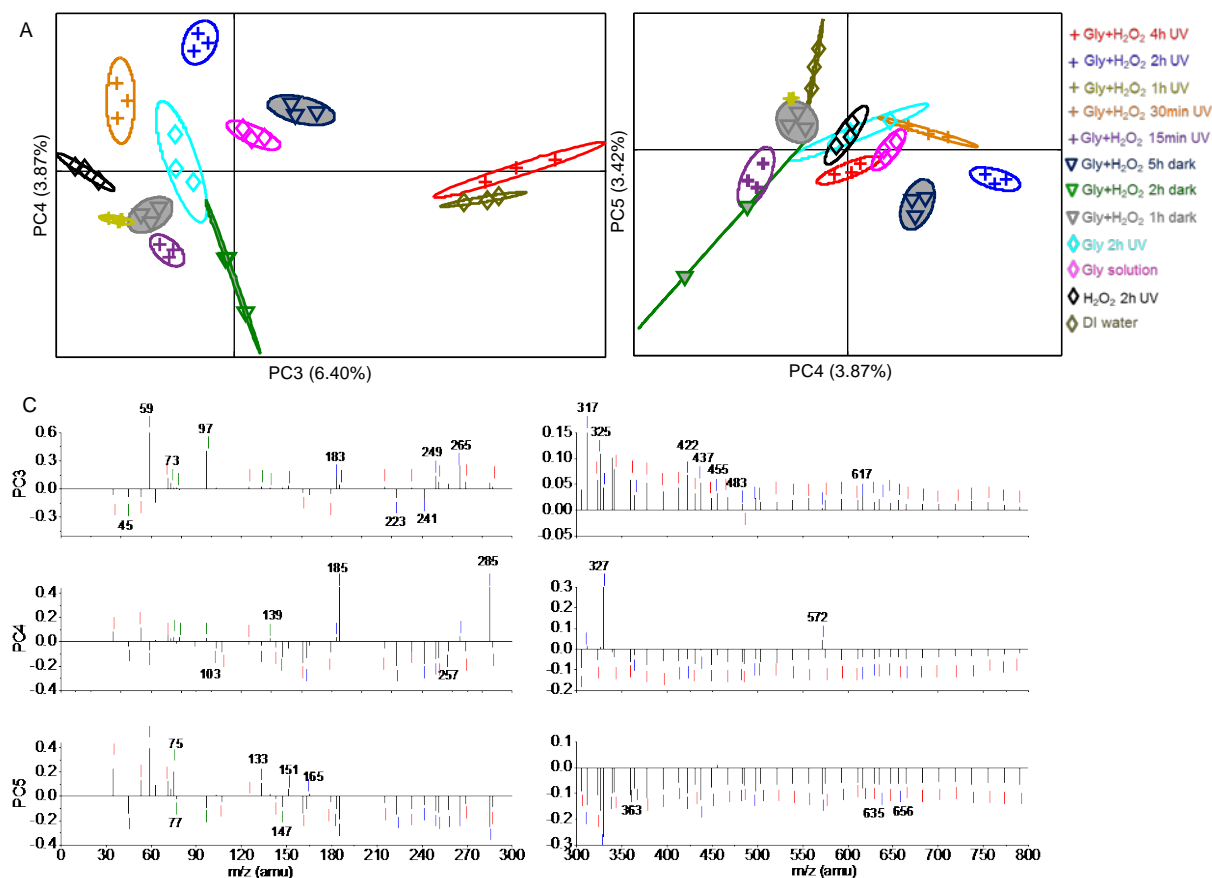
Figure S12. Selected peaks of spectral PCA analysis in the negative mode (normalized to the total of the selected ions). (A) Score plot of PC3 vs. PC4. (B) Score plot of PC4 vs. PC5. (C) Loading plots of PC2, PC3, PC4 and PC5.

Other selected peaks PCA results in negative mode were shown in Figure S12 to support the results in Figure 4 in the main text; each PC loading plot shows the important m/z peaks that contribute to differentiation among samples.
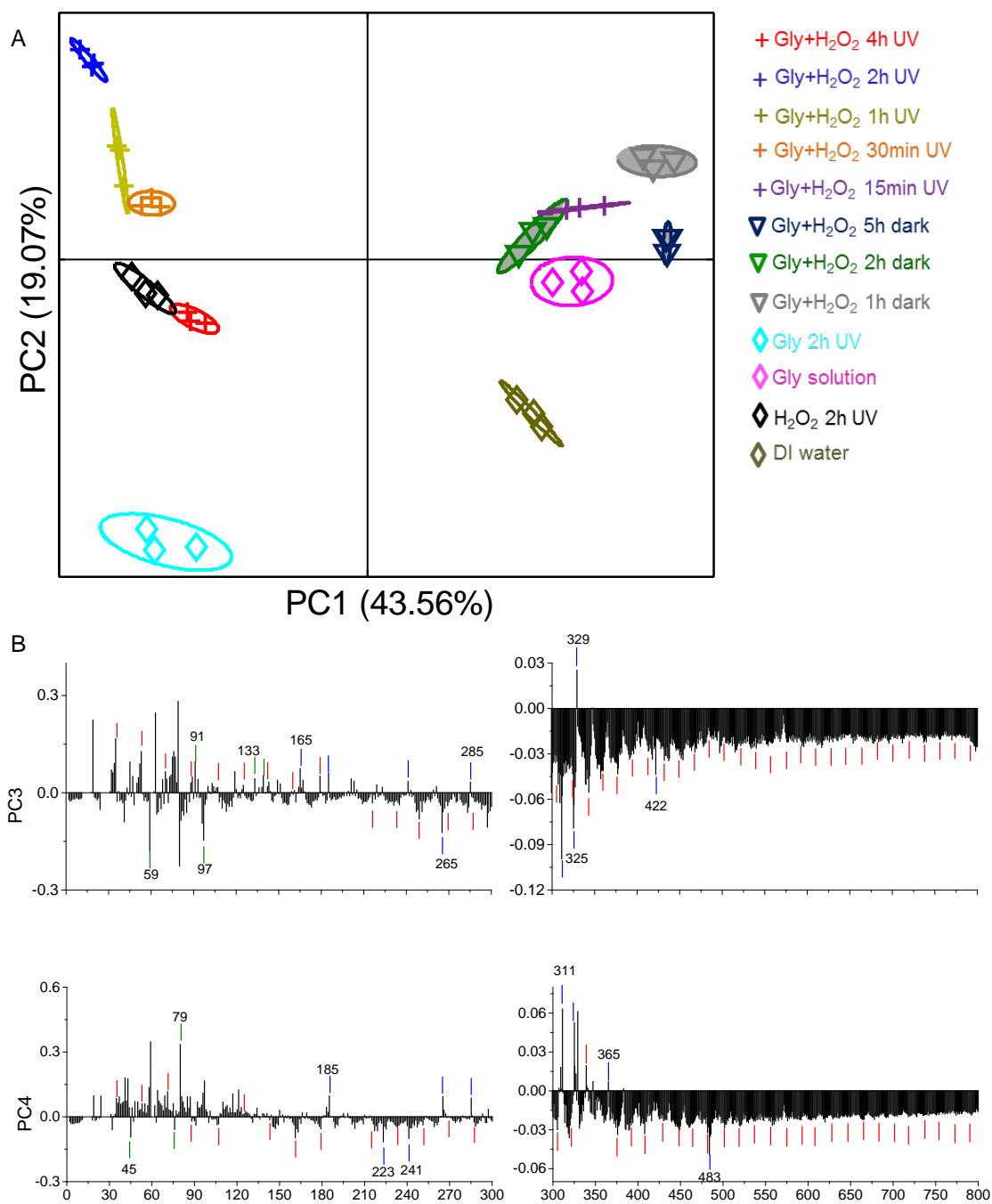
Figure S13. All peaks positive spectral PCA analysis (normalized to total ions). (A) Score plot of PC1 vs. PC2. (B) Loading plots of PC1 and PC2.

The spectral PCA analysis of all peaks was done before the selected peaks PCA to understand the data and facilitate peak selection. The positive mode results are shown in Figure S13.
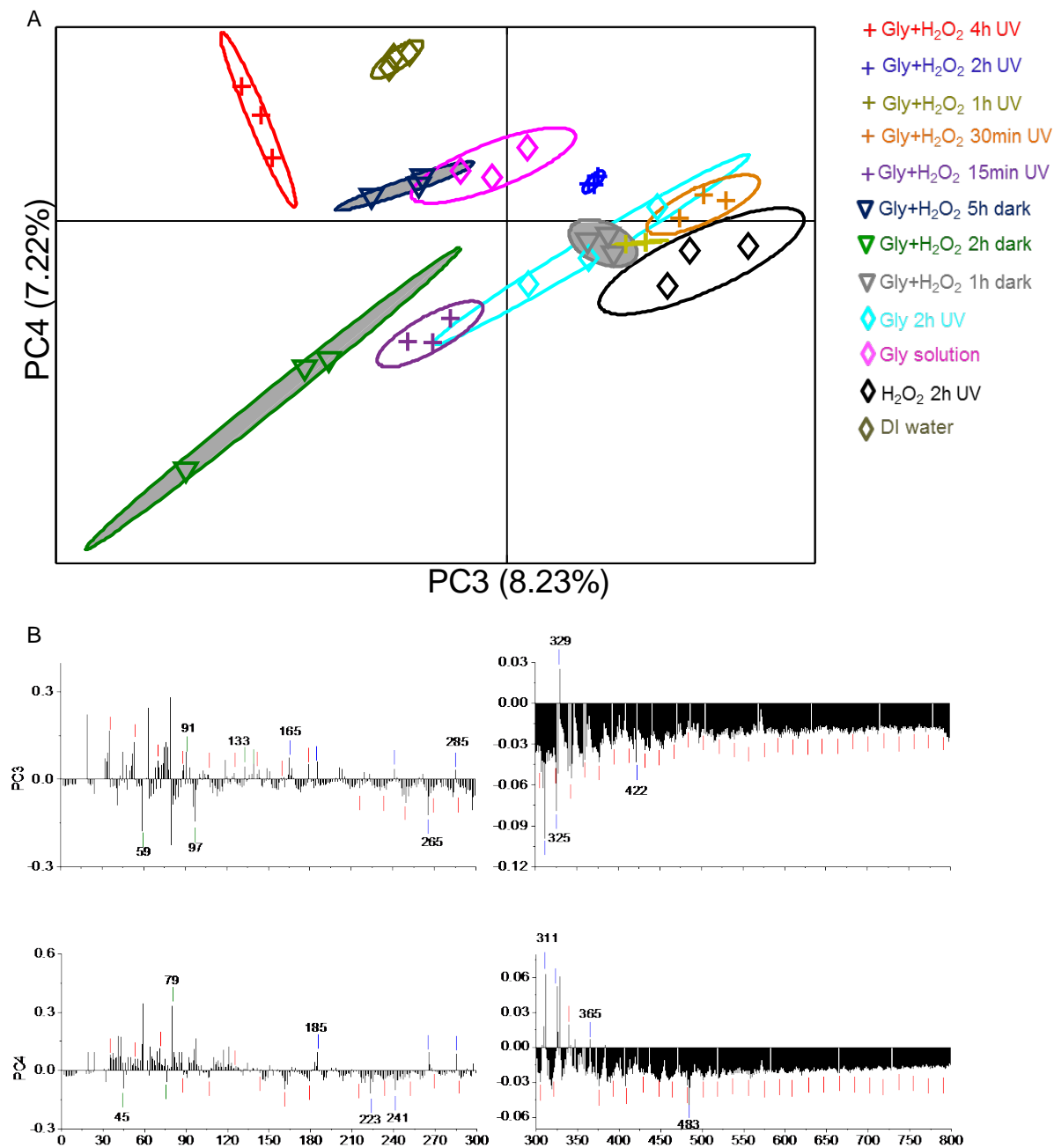
Figure S14. All peaks negative spectral PCA analysis (normalized to total ions5. (A) Score plot of PC3 vs. PC4. (B) Loading plots of PC3 and PC4.

Similarly, the negative all peak spectral PCA results were depicted in Figure S14. All peaks PCA showed that 2 hr. UV was similar to that of dark reactions; however, 2 hr. UV and 4.hr. UV were different. Important peaks contributing to the score plot of PC1 vs.PC5 were used as the base in the selected peak spectral PCA analysis. Specifically, selected peaks include oxidation products (e.g., formic acid, m/z$^-$ 45, tartaric acid, m/z$^-$ 149 H_2O...HCO_3^- anion, m/z$^-$ 79); oligomers (e.g., oligomerm/z$^+$ 327 in the positive mode; m/z$^-$ 422 in the negative mode); cluster ions (i.e., tartaric acid…glyoxylic acid…formic acid…H_2O, m/z 285 in the negative mode) and water clusters observed in both the positive and negative mode.
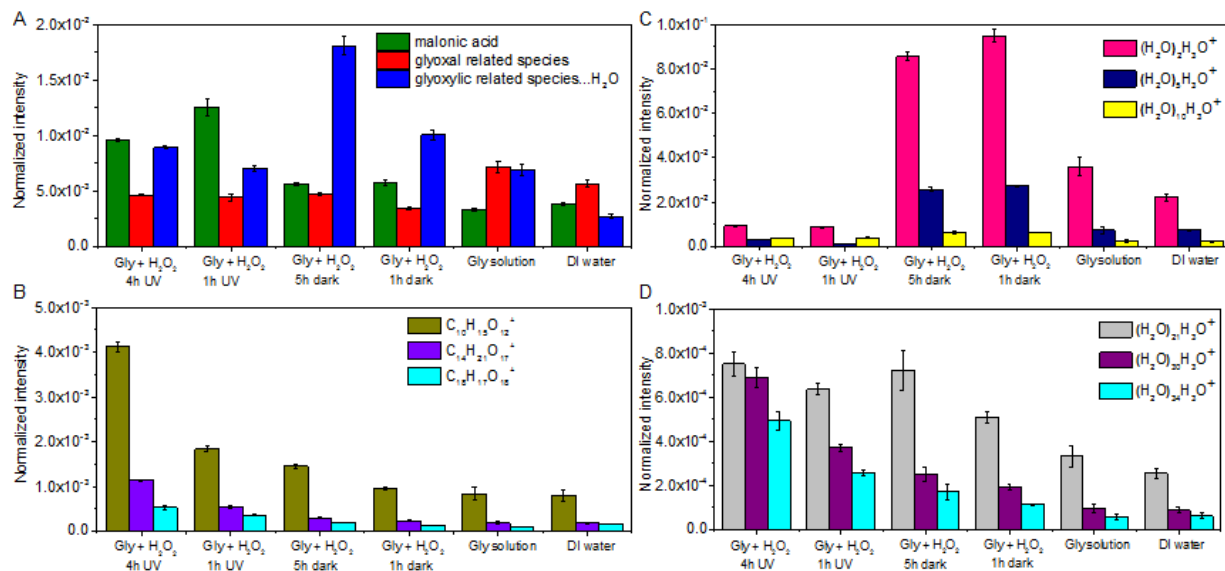
Figure S15. Comparison of of key oxidization products, glyoxal-trace peaks, oligomers and water clusters in the positive mode (normalized to the total counts of the selected ions): (A) Oxidiation products in the positive mode. (B) Oligomers in the positive mode. (C) Small water clusters in the positive mode. (D) Large water clusters in the positive mode.
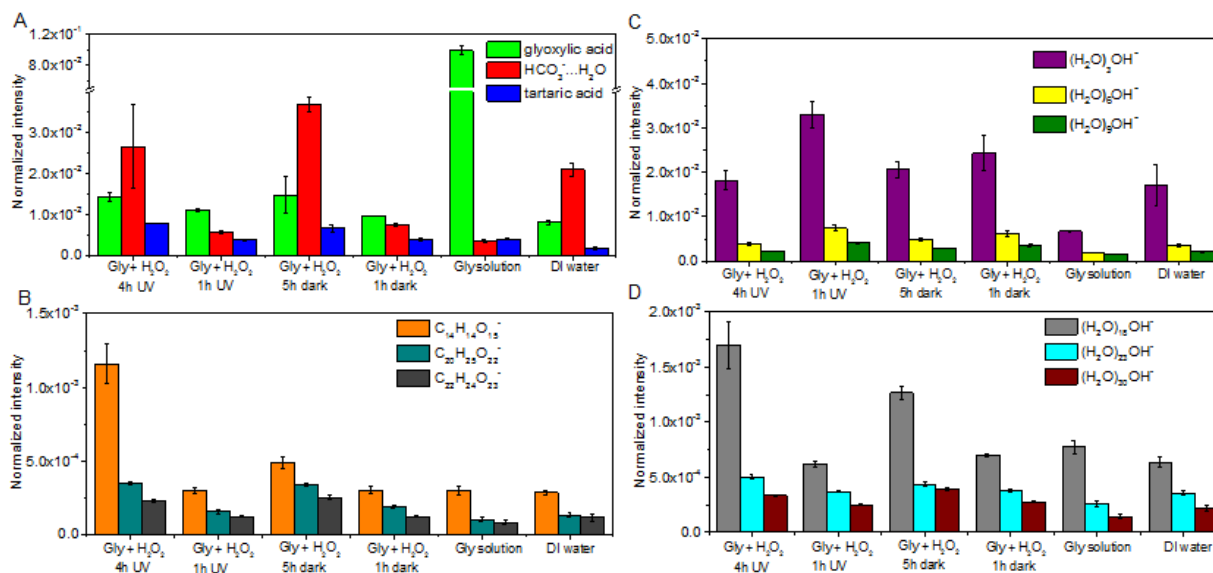
Figure S16. Comparison of of key oxidization products, oligomers and water clusters in the negative mode (normalized to the total counts of the selected ions): (A) Oxidiation products in the negative mode. (B) Oligomers in the negative mode. (C) Small water clusters in the negative mode. (D) Large water clusters in the negative mode.

In order to study the difference of glyoxal oxidation products, bar plots of key oxidization products, oligomers and water clusters both in positive and negative mode were shown in Figures S15 & S16. Data were normalized to the selected total ions in both the positive and negative mode. Malonic acid (m/z^+ 105) had high intensity among UV samples. Short-time dark reactions had lower counts in oxidation product peaks, control sample had even lower counts in products, implying that UV processing and aging time could influence the degree of glyoxal oxidation. In comparison with photochemical reactions, more $H_2O...HCO_3$ (m/z^- 79, $CH_3O_4^-$) anion was observed in the 4 hr. UV and 5 hr. dark sample, suggesting that glyoxal could be oxidized to CO_2 given longer reaction time. Also, glyoxylic acid was another important product in both dark and photochemical pathways, which had high intensity in all mixed samples. In Figures S15b and S16b, more oligomers were observed in the UV exposed sample. Complimentary to this finding, oligomers in the negative mode were more likely to form under long-time UV condition and dark reactions.

Water clusters were another interesting and important observation (Figures S15a, b and S16a, b). The water microenvironment changed depending on reaction time and conditions. Photochemical aging seemed to have different water affinity that contains larger water clusters, while small water clusters were more likely encountered in dark reactions than UV associated reactions. The bar plots showed similar characteristics with PCA results. Under UV conditions, oligomer formation was an essential pathway that contributes to SOA formation. In dark conditions, aqueous surface reactions could also contribute to the aqSOA formation supported by the production of carboxylic acids and oligomers. Second, small clusters ($n \leq 9$) were more likely to form under dark reactions, and larger water clusters were more prominent under UV reactions.
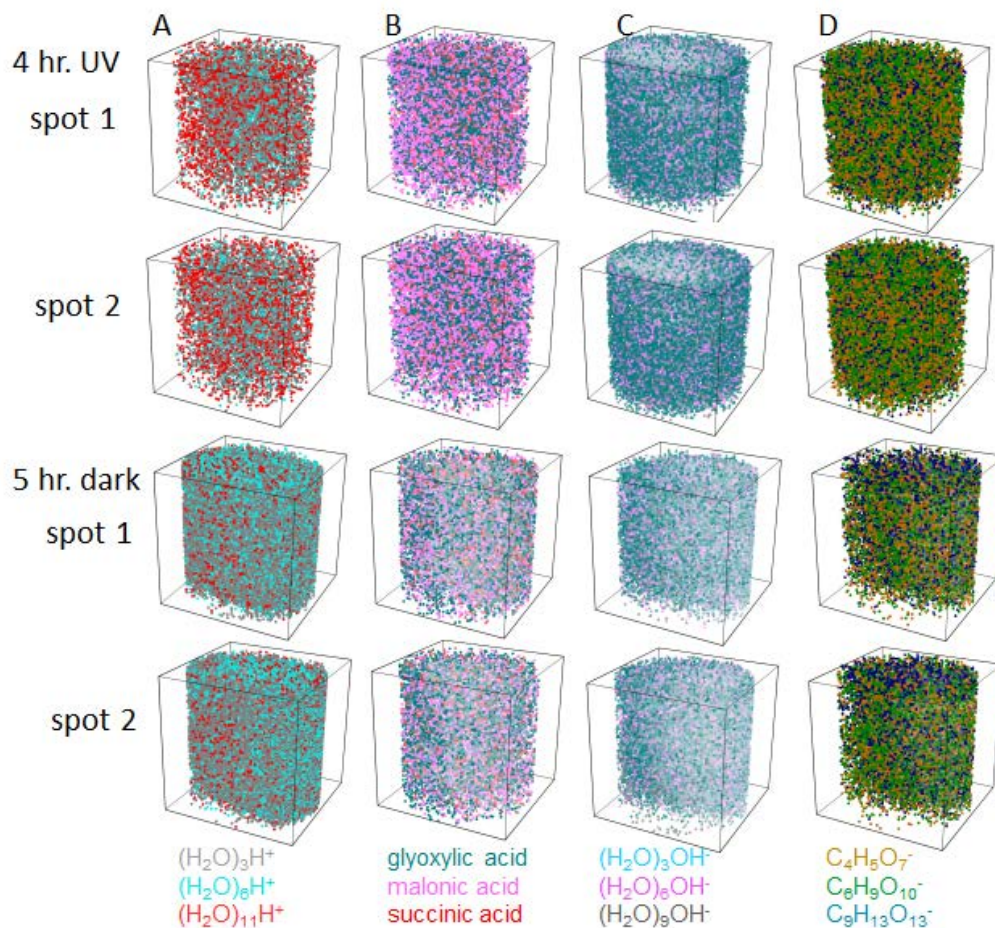
Figure S17. 3D image Comparison of key oxidization products, oligomers and water clusters in the positive mode from 4 hr. photochemical aging and 5 hr. dark reactions showing m/z peaks of (A) small water clusters, (B) carboxylic acid and hydration products, (C) carboxylic acid (D) oligomers and cluster ions, (E) oligomers, and (F) large water clusters.

Beside the reconstructed 3D images shown in Figure 6, replicate 3D image plots in the positive mode are shown in Figure S17. The distribution of these ions is consistent among different spots, indicating that that good reproducibility of liquid SIMS 3D image analysis.
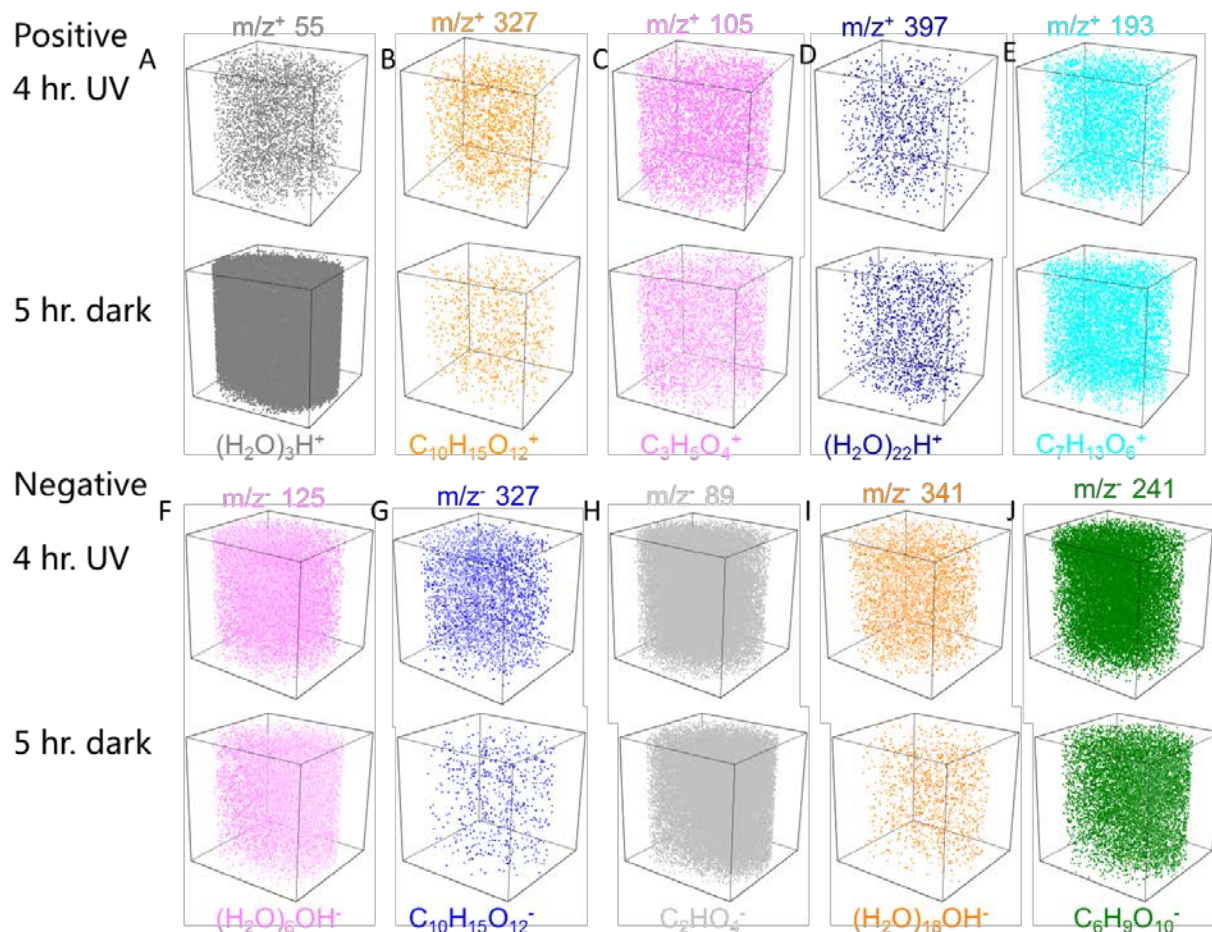
Figure S18. 3D images of individual components in both positive and negative mode of key products (normalized to total ions) from 4 hr. photochemical aging and 5 hr. dark reactions of (A) small water clusters, (B) oligomers, (C) carboxylic acids, (D) large water clusters, (E) cluster ions and negative mode of key products of (F) small water clusters, (G) oligomers, (H) carboxylic acids, (I) large water clusters, (J) cluster ions.

Figure S18 depicts individual component spatial distribution. This is an alternative manner to illustrate the 3D mixing state as shown in Figure 6. UV photochemical reactions produce higher intensities of oligomers (i.e., m/z$^+$ 327, $C_{10}H_{15}O_{12}^+$, m/z$^-$ 327, $C_{10}H_{15}O_{12}^-$), carboxylic acids (i.e., m/z$^+$ 105, $C_3H_5O_4^+$, m/z$^-$ 89, $C_2HO_4^-$) and cluster ions (i.e., m/z$^+$ 193, $C_7H_{13}O_6^+$, m/z$^-$ 241, $C_6H_9O_{10}^-$) than dark aging. The small water clusters (i.e., m/z$^+$ 55, $(H_2O)_3H^+$, m/z$^-$ 125, $(H_2O)_6OH^-$) have higher intensity in dark aging than those in the UV aging. For the large water clusters (i.e., m/z$^-$ 341, $(H_2O)_{18}OH^-$), they are more favourably formed in the UV aging.

24
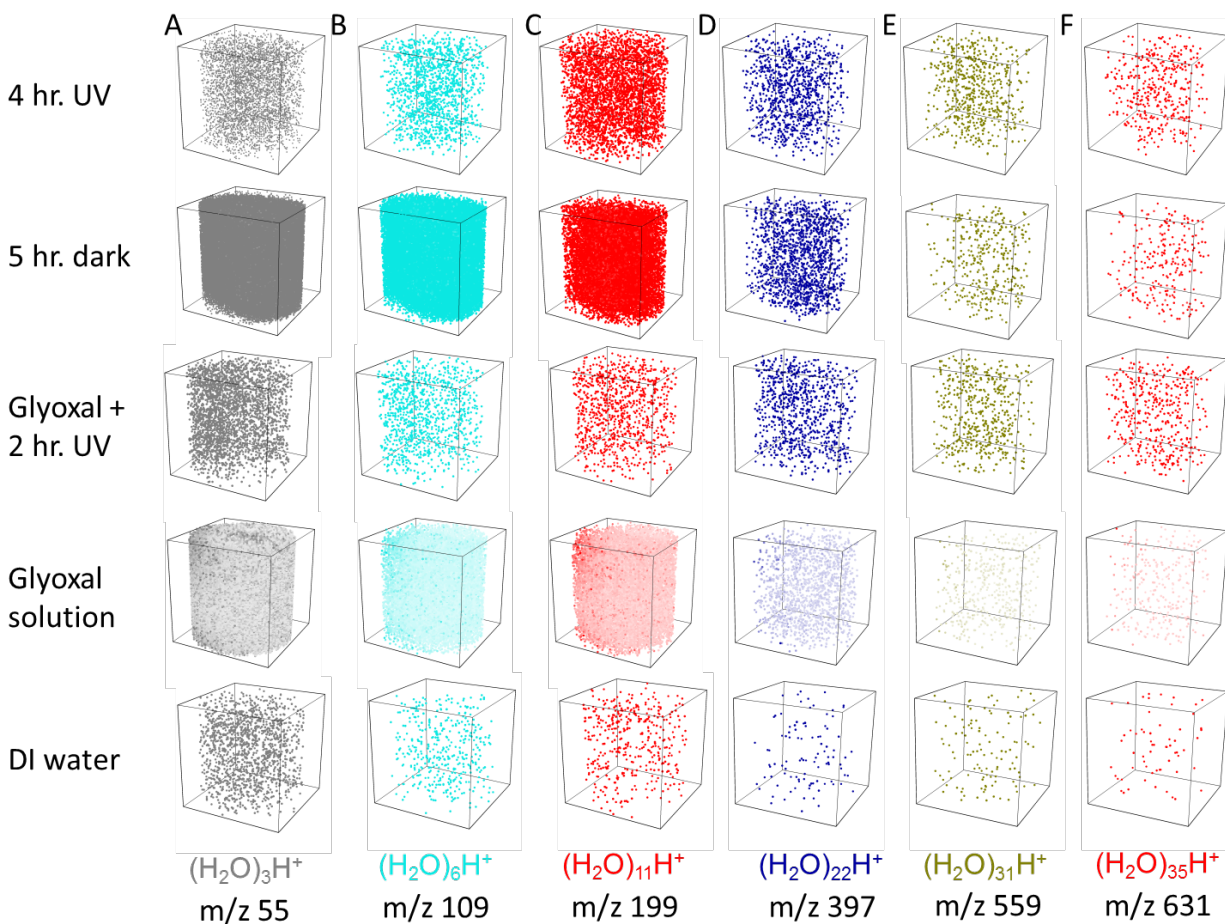
Figure S19a. 3D images of water clusters (normalized to total ions) from 4 hr. photochemical aging, 5 hr. dark reactions, glyoxal with 2hr. UV, glyoxal solution and DI water samples in the positive mode: A) m/z$^+$ 55, $(H_2O)_3H^+$, B) m/z$^+$ 109, $(H_2O)_6H^+$, C) m/z$^+$ 199, $(H_2O)_{11}H^+$, D) m/z$^+$ 397, $(H_2O)_{22}H^+$; E) m/z$^+$ 559, $(H_2O)_{31}H^+$; and F) m/z$^+$ 631, $(H_2O)_{35}H^+$.

Figure S19a shows the change of the water clusters in the positive ion mode on the surface, indicating the change of hydrophobicity/hydrophilicity of the aqueous microenvironment. Water clusters observed in the UV aging and dark aging sample surfaces are different from three different controls including glyoxal with 2 hr. UV illumination, glyoxal solution, and DI water. The water clusters in 4 hr. UV aging have higher intensity than those in the glyoxal solution and DI water controls. Small water clusters (i.e., m/z$^+$ 55, $(H_2O)_3H^+$, m/z$^+$ 109, $(H_2O)_6H^+$ and m/z$^+$ 199, $(H_2O)_{11}H^+$) tend to form in dark aging. Large water clusters (i.e., m/z$^+$ 397, $(H_2O)_{22}H^+$; m/z$^+$ 559, $(H_2O)_{31}H^+$; and m/z$^+$ 631, $(H_2O)_{35}H^+$) are more likely to more in the UV photolysis process.
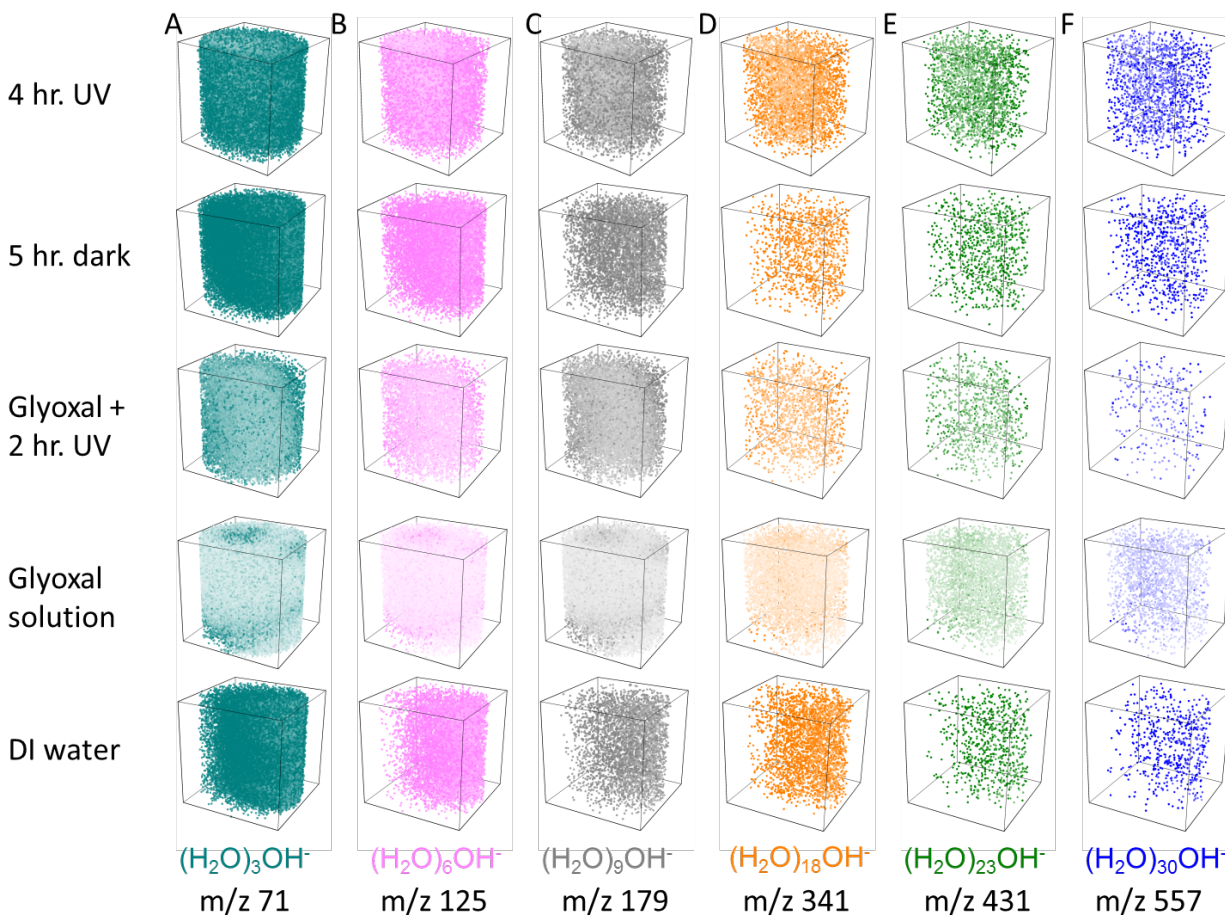
Figure S19b. 3D images of water clusters (normalized to total ions) from 4 hr. photochemical aging, 5 hr. dark reactions, glyoxal with 2hr. UV, glyoxal solution and DI water samples in the negative mode: A) m/z$^-$ 71, $(H_2O)_3OH^-$ B) m/z$^-$ 125, $(H_2O)_6OH^-$, C) m/z$^-$ 179, $(H_2O)_9OH^-$, D) m/z$^-$ 341, $(H_2O)_{18}OH^-$, E) m/z$^-$ 431, $(H_2O)_{23}OH^-$, and F) m/z$^-$ 557, $(H_2O)_{30}OH^-$.

The water clusters formed under the UV photochemical aging and dark reactions differ from the three control samples (i.e., glyoxal solution with 2 hr. UV, glyoxal solution and DI water) in the negative mode as shown in Figure. S19b. The 4 hr. UV aging and 5 hr. dark aging have distinct water cluster spatial distribution compared with the two glyoxal controls, indicating that the hydrogen peroxide indeed participates in the reactions and has an influence on the aqueous surface hydrophobicity. Similarly to the positive mode, the small water clusters (i.e., m/z$^-$ 71, $(H_2O)_3OH^-$; m/z$^-$ 125, $(H_2O)_6OH^-$; m/z$^-$ 179, $(H_2O)_9OH^-$) tend to form in dark aging, while the larger water clusters (i.e., m/z$^-$ 341, $(H_2O)_{18}OH^-$; m/z$^-$ 431, $(H_2O)_{23}OH^-$; m/z$^-$ 557, $(H_2O)_{30}OH^-$) are more likely to form in the presence of UV photolysis.

Supplementary Tables

Table S1a. Product summary of glyoxal + H_2O_2 reaction under different conditions in the positive mode.

products	glyoxal + H_2O_2 + hv	glyoxal + H_2O_2 dark
hydration	$C_2H_7O_3^+$	$C_2H_7O_3^+$
carboxylic acid	$C_2H_3O_3^+$	
	$C_2H_5O_3^+$	
	$C_3H_5O_4^+$	
oligomer	$C_6H_9O_7^+$	$C_6H_9O_7^+$
	$C_6H_{10}O_7^+$	
	$C_6H_9O_9^+$	$C_6H_9O_9^+$
	$C_8H_9O_{11}^+$	$C_8H_9O_{11}^+$
	$C_8H_9O_{11}^+$	
	$C_9H_{17}O_{12}^+$	
	$C_8H_{15}O_{13}^+$	
	$C_{12}H_{17}O_{15}^+$	
	$C_{13}H_{23}O_{16}^+$	
	$C_{14}H_{21}O_{17}^+$	$C_{14}H_{21}O_{17}^+$
	$C_{18}H_{17}O_{18}^+$	
	$C_{19}H_{31}O_{24}^+$	
cluster ion	$C_8H_{15}O_8^+$	
	$C_9H_{17}O_{12}^+$	

Table S1b. Product summary of glyoxal + H_2O_2 reaction under different conditions in the negative mode.

products	glyoxal + H_2O_2 + $h\nu$	glyoxal + H_2O_2 dark
hydration	$C_2H_5O_3^-$	$C_2H_5O_3^-$
	$C_2H_3O_4^-$	
carboxylic acid	CHO_2^-	CHO_2^-
	$C_2HO_3^-$	
	$C_2H_3O_3^-$	
	$CH_3O_4^-$	$CH_3O_4^-$
	$C_2HO_4^-$	$C_2HO_4^-$
	$C_3H_3O_4^-$	
	$C_4H_5O_5^-$	
	$C_4H_5O_6^-$	
oligomer	$C_6H_7O_9^-$	$C_6H_7O_9^-$
	$C_8H_9O_9^-$	
	$C_6H_9O_{11}^-$	$C_6H_9O_{11}^-$
	$C_8H_9O_{10}^-$	$C_8H_9O_{10}^-$
	$C_6H_5O_{12}^-$	
	$C_8H_{13}O_{11}^-$	$C_8H_{13}O_{11}^-$
	$C_9H_{11}O_{12}^-$	$C_9H_{11}O_{12}^-$
	$C_{10}H_{19}O_{14}^-$	
	$C_{14}H_{14}O_{15}^-$	
	$C_{12}H_{21}O_{17}^-$	$C_{12}H_{21}O_{17}^-$
	$C_{12}H_{23}O_{18}^-$	
	$C_{13}H_{23}O_{19}^-$	
	$C_{18}H_{20}O_{21}^-$	
	$C_{20}H_{25}O_{22}^-$	$C_{20}H_{25}O_{22}^-$
	$C_{22}H_{19}O_{22}^-$	
	$C_{22}H_{24}O_{23}^-$	
cluster ion	$C_4H_5O_7^-$	$C_4H_5O_7^-$
	$C_4H_7O_8^-$	
	$C_4H_9O_8^-$	$C_4H_9O_8^-$
	$C_6H_9O_{10}^-$	$C_6H_9O_{10}^-$
	$C_{10}H_{13}O_{12}^-$	$C_{10}H_{13}O_{12}^-$
	$C_9H_{13}O_{13}^-$	$C_9H_{13}O_{13}^-$

Table S2. Summary of sample and experimental conditions.

Exp. No.	Initial composition*	UV or dark treatment	Treatment time	pH
1	Gly and H_2O_2	dark	1 hr.	4.33
2	Gly and H_2O_2	dark	2 hr.	4.15
3	Gly and H_2O_2	dark	5 hr.	4.09
4	Gly and H_2O_2	UV	0.25 hr.	3.84
5	Gly and H_2O_2	UV	0.5 hr.	3.88
6	Gly and H_2O_2	UV	1 hr.	3.74
7	Gly and H_2O_2	UV	2 hr.	3.58
8	Gly and H_2O_2	UV	4 hr.	3.8
9	H_2O_2	UV	2 hr.	8.45
10	Gly	UV	2 hr.	7.22
11	Gly	neither UV nor dark		4.49
12	DI water	neither UV nor dark		6.99

*Gly = 5 mM glyoxal solution;H_2O_2 = 20 mM hydrogen peroxide solution.

In order to exclude uncertain factors of solution and instrument, 12 samples were set up to study aqueous surface glyoxal oxidation products, shown in Table S2, five UV, three dark reactions and four control samples were included in the experiment schedule. Namely, various controls including UV, glyoxal, H_2O_2, and deionized (DI) water were analyzed. Glyoxal (Fisher scientific, 40% wt. solution in water, grade: electrophoresis), hydrogen peroxide (H_2O_2), (Fisher scientific, 30% wt. solution in water, certified ACS) and DI water (18.2 MΩ) dispensed from a Barnstead water purification system (Model: Nanopure diamond) were used. Before an experiment, the pH of each solution was determined using a pH meter (ORION pH meter, 410A).

Table S3a. Representative peaks used in selected peak spectral PCA in the positive mode including oxidation products, cluster ions, and oligomers

m/z	suggest formula	suggest structure	possible assignment	ref
59	$C_2H_3O_2^+$	$(CHOCHO)H^+$	$[glyoxal+H]^+$	[9]
75	$C_2H_3O_3^+$	$(CHOCOOH)H^+$	$[glyoxylic\ acid+H]^+$	[10]
77	$C_2H_5O_3^+$	$(CH_2OHCOOH)H^+$	$[monohydrated\ glycolic\ acid+H]^+$	[10]
79	$C_2H_7O_3^+$	$((CH_2OH)_2)H^+$	$[hydrated\ glycolaldehyde+H]^+$	[10]
105	$C_3H_5O_4^+$	$(HOOCCH_2COOH)H^+$	$[malonic\ acid+H]^+$	[11]
117	$C_4H_5O_4^+$	$(CHOCHO)_2H^+$	$[monohydrated\ glyoxaldimer+H]^+$	[1]
119	$C_4H_7O_4^+$	$(HOOCCH_2CH_2COOH)H^+$	$[succinic\ acid+H]^+$	[12]
131	$C_5H_7O_4^+$	$(HOOC(CH)_2CH_2COOH)H^+$	$[glyoxal\ related\ species]^+$	[13]
149	$C_5H_9O_5^+$	$(HOOC(CH)_2CH_2COOH)H^+…H_2O$	$[m/z\ 131…H_2O]^+$	[14]
193	$C_6H_9O_7^+$	$(C_2H_4O_3......C_4H_4O_4)H^+$	$[oligomer+H]^+$	This study
194	$C_6H_{10}O_7^+$	$((CHOCHO)_2CH(OH)_2CHOH)H^+$	$[oligomer+H]^+$	[15]
225	$C_6H_9O_9^+$	$((CHOCOOH)_2CH_2(OH)COOH)H^+$	$[oligomer+H]^+$	[14]
193	$C_7H_{13}O_6^+$	$((CHOCOOH)_2CH_2(OH)COOH)H^+$	$[oligomer+H]^+$	[14]
239	$C_8H_{15}O_8^+$	$(C_7H_{12}O_6......HCOOH)H^+$	$[m/z\ 193......formic\ acid]^+$	This study
281	$C_8H_9O_{11}^+$	$(CHOCOOH)_3......CHOCHO)H^+$	$[oligomer+H]^+$	[14]
285	$C_8H_{13}O_{11}^+$	$((CHOCOOH)_3......(CH_2OH)_2)H^+$	$[oligomer+H]^+$	[14]
317	$C_9H_{17}O_{12}^+$	$(C_7H_{10}O_9......C_2H_6O_3)H^+$	$[m/z\ 239......\ dehydratedglyoxal]^+$	This study
319	$C_8H_{15}O_{13}^+$	$(CHOCOOH)_3......(HCHO)_2)H^+......2H_2O$	$[oligomer+H]^+$	This study
327	$C_{10}H_{15}O_{12}^+$	$((CHOCHO)_4CH(OH)_2CH(OH)_2)H^+$	$[oligomer+H]^+$	[15]
401	$C_{12}H_{17}O_{15}^+$	$(C_{10}H_{14}O_{12}......CHOCOOH)H^+$	$[oligomer+H]^+$	This study
435	$C_{13}H_{23}O_{16}$	$(C_9H_{19}O_{12}......C_4H_4O_4)H^+$	$[oligomer+H]^+$	This study
461	$C_{14}H_{21}O_{17}^+$	$((CHOCHO)_6CH(OH)_2CH(OH)_2)H^+...H_2O$	$[oligomer+H]^+$	This study
521	$C_{18}H_{17}O_{18}^+$	$(\ (CHOCHO)_4COCO(CHOCHO)_4)H^+$	$[oligomer+H]^+$	This study
643	$C_{19}H_{31}O_{24}^+$	$(C_{10}H_{14}O_{12}......C_9H_{16}O_{12})H^+$	$[oligomer+H]^+$	This study

Notes: [a]: ……: Van der Waals force; [b]…: hydrogen bond

Important peaks selected in the positive PCA spectral analysis were listed in Table S4a. Peaks used in the selected PCA analysis were selected based on the following criteria: 1) The peak intensity was more than

3% of the total ion counts before m/z 100 and more than 0.5% of total ions after m/z 100; 2) S/N ratio is at least 3.0; 3) peaks representing important reaction products based on literature; 4) Peaks contributing to the differentiation in all peak PCA loading plots, loadings should be at least 3 times higher than their neighbors; 5) All water cluster peaks in both the negative and positive mode (seen in Table 1b and Table 2b); and 6) PDMS interference, Bi^+ and system interference peaks are excluded (summarized in Figures S5a and S6b.

Table S3b. Representative peaks used in selected peak spectral PCA in the negative mode including oxidation products, cluster ions, and oligomers.

m/z	suggest formula	suggest structure	possible assignment	ref
45	CHO_2^-	$HCOO^-$	[formic acid-H]$^-$	[10]
59	$C_2H_3O_2^-$	CH_3COO^-	[acetic acid-H]$^-$	[10]
73	$C_2HO_3^-$	$CHOCOO^-$	[glyoxylic acid-H]$^-$	[10]
75	$C_2H_3O_3^-$	$CH_2(OH)COO^-$	[monohydrated glyoxal/glycolic acid-H]$^-$	[10]
77	$C_2H_5O_3^-$	$CH(OH)_2CH(OH)^-$	[glycolaldehyde dimer-H]$^-$	[10]
79	$CH_3O_4^-$	$H_2O...HCO_3^-$	[$H_2O...HCO_3$]$^-$	[10]
89	$C_2HO_4^-$	$HOOCCOO^-$	[oxalic acid-H]$^-$	[10]
91	$C_2H_3O_4^-$	$CH(OH)_2COOH$	[monohydrated glyoxylic acid-H]$^-$	[10]
97	$CH_5O_5^-$	$2H_2O...HCO_3^-$	[$2H_2O...HCO_3$]$^-$	[10]
103	$C_3H_3O_4^-$	$HOOCCH_2COO^-$	[malonic acid-H]$^-$	[11]
133	$C_4H_5O_5^-$	$HOOCCH_2CHOHCOO^-$	[malic acid-H]$^-$	[14, 19]
149	$C_4H_5O_6^-$	$HOOCCH_2CH(OH)_2COO^-$	[tartaric acid-H]$^-$	[11]
151	$C_4H_7O_6^-$	$CHOCH_2(OH)......CHOCOO^-...H_2O$	[oligomer-H]$^-$	This study
163	$C_4H_3O_7^-$	$COOHCHCOOHOCOO^-$	[hydroxymethanetricarboxylic acid-H]$^-$	This study
165	$C_4H_5O_7^-$	$HOOCCOOH...CH_2OHCOO^-$	[$HOOCCOOH...CH_2OHCOO^-$]$^-$	This study
183	$C_4H_7O_8^-$	$HOOCCOOH...CH_2OHCOO^-...H_2O$	[m/z 165...H_2O]$^-$	This study
185	$C_4H_9O_8^-$	$CHOCHO......CHOCOO^-...3H_2O$	[oligomer-H]$^-$	This study
223	$C_6H_7O_9^-$	$C_4H_6O_6......CHOCOO^-$	[oligomer-H]$^-$	[14]
241	$C_6H_9O_{10}^-$	$C_4H_6O_6......CHOCOO^-...H_2O$	[m/z 223...H_2O]$^-$	This study
249	$C_8H_9O_9^-$	$(CHOCHO)_3CHOCH(OH)O^-$	[oligomer-H]$^-$	[15]
257	$C_6H_9O_{11}^-$	$C_6H_9O_{11}^-$	[oligomer-H]$^-$	This study
265	$C_8H_9O_{10}^-$	$(CHOCH_2(OH))_2......COCOOHCOCOO^-$	[cluster ion]$^-$	This study
269	$C_6H_5O_{12}^-$	$(HOOCCOOH)_2HOOCCOO^-$	[oxalic acid trimer-H]$^-$	This study
285	$C_8H_{13}O_{11}^-$	$(CHOCHO)_3CH(OH)_2CH(OH)O^-...H_2O$	[oligomer-H]$^-$	This study
311	$C_9H_{11}O_{12}^-$	$C_8H_9O_{10}^-......HCOOH$	[oligomer-H]$^-$	This study
325	$C_{10}H_{13}O_{12}^-$	$C_8H_9O_{10}^-......CHOCH_2(OH)$	[m/z 265...monohydrated glyoxal]$^-$	This study

m/z	suggest formula	suggest structure	possible assignment	ref
329	$C_9H_{13}O_{13}^-$	$C_8H_9O_{10}^-$......$HCOOH$...H_2O	[m/z 311 … H_2O]$^-$	This study
363	$C_{10}H_{19}O_{14}^-$	$C_8H_9O_{10}^-$......$CH_2OHCH(OH)_2$...$2H_2O$	[oligomer-H]$^-$	This study
422	$C_{14}H_{14}O_{15}^-$	$(CHOCHO)_6COC(OH)_2^-$	[oligomer-H]$^-$	[15]
437	$C_{12}H_{21}O_{17}^-$	$(CHOCHO)_5CH(OH)_2CH(OH)O^-$ ...$3H_2O$	[oligomer-H]$^-$	This study
455	$C_{12}H_{23}O_{18}^-$	$(CHOCHO)_5CH(OH)_2CH(OH)O^-$ ...$4H_2O$	[oligomer-H]$^-$	This study
483	$C_{13}H_{23}O_{19}^-$	$C_{12}H_{21}O_{17}^-$......$HCOOH$	[oligomer-H]$^-$	This study
572	$C_{18}H_{20}O_{21}^-$	$C_4H_6O_6$......$(CHOCHO)_6COC(OH)_2^-$	[oligomer-H]$^-$	This study
617	$C_{20}H_{25}O_{22}^-$	$(CHOCHO)_8(CHOCH_2OH)CH(OH)_2CH(OH)O^-$	[oligomer-H]$^-$	This study
635	$C_{22}H_{19}O_{22}^-$	$(CHOCHO)_5COCO(CHOCHO)_4CHOCO^-$	[oligomer-H]$^-$	This study
656	$C_{22}H_{24}O_{23}^-$	$(CHOCHO)_{10}CH_2OCH(OH)O^-$	[oligomer-H]$^-$	This study

Notes: [a]: ……: Van der Waals force; [b] …: hydrogen bond

Important peaks selected based on previous criteria in the negative spectral PCA were listed in Table S4b.

Table S4a Comparison of main oxidation products in the positive mode.

Species	Formula	Unit mass	Theoretical mass	Observed mass
Tartaric acid+H	$C_4H_7O_6^+$	151	151.024	151.032
Succinic acid+H	$C_4H_7O_4^+$	119	119.034	119.058
Malonic acid+H	$C_3H_5O_4^+$	105	105.019	105.014
Malic acid+H	$C_4H_7O_5^+$	135	135.029	135.142
Oxalic acid+H	$C_2H_3O_4^+$	91	91.003	91.105
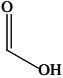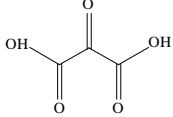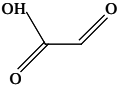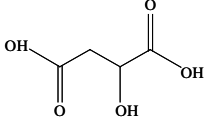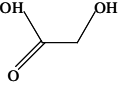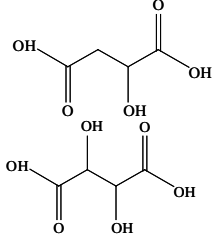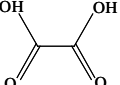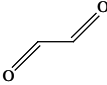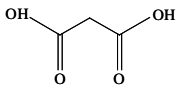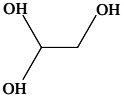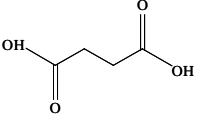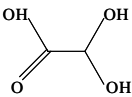
Table S4b Comparison of main oxidation products in the negative mode.

Species	Formula	Unit mass	Theoretical mass	Observed mass
Tartaric acid-H	$C_4H_5O_6^-$	149	149.009	149.007
Succinic acid-H	$C_4H_5O_4^-$	117	117.019	116.974
Malonic acid-H	$C_3H_3O_4^-$	103	103.003	103.016
Malic acid-H	$C_4H_5O_5^-$	133	133.014	133.034
Oxalic acid-H	$C_2HO_4^-$	89	88.987	88.980

Peak identification and comparison using high mass resolution (five dry reference samples (oxalic acid, malonic acid, succinic acid, malic acid and tartaric acid) and unit mass (liquid sample) were listed in Table S2. Unit mass, theoretical mass and observed mass are consistent show that the liquid SIMS unit mass identifications of key products are reliable.

Supporting Information

Table S4c.Chemical structure of key representative products and reactants.

species	structure	species	structure
formic acid		mesoxalic acid	
glyoxylic acid		malic acid	
glycolic acid		tartaric acid	
oxalic acid		glyoxal molecule	
malonic acid		glycolaldehyde hydrated	
succinic acid		hydrated form of glyoxalic acid	

The chemical structures of key products are provided to assist discussions in the main text.

Table S5a. Water cluster peaks in the positive mode.

m/z	formula	notes	ref
19	$(H_2O)H^+$	[water cluster+H] $^+$	[16-18]
37	$(H_2O)_2H^+$		
55	$(H_2O)_3H^+$		
73	$(H_2O)_4H^+$		
91	$(H_2O)_5H^+$		
109	$(H_2O)_6H^+$		
127	$(H_2O)_7H^+$		
145	$(H_2O)_8H^+$		
163	$(H_2O)_9H^+$		
181	$(H_2O)_{10}H^+$		
199	$(H_2O)_{11}H^+$		
217	$(H_2O)_{12}H^+$		
235	$(H_2O)_{13}H^+$		
253	$(H_2O)_{14}H^+$		
271	$(H_2O)_{15}H^+$		
289	$(H_2O)_{16}H^+$		
307	$(H_2O)_{17}H^+$		
325	$(H_2O)_{18}H^+$		
343	$(H_2O)_{19}H^+$		
361	$(H_2O)_{20}H^+$		
379	$(H_2O)_{21}H^+$		
397	$(H_2O)_{22}H^+$		
415	$(H_2O)_{23}H^+$		
433	$(H_2O)_{24}H^+$		
451	$(H_2O)_{25}H^+$		
469	$(H_2O)_{26}H^+$		
487	$(H_2O)_{27}H^+$		
505	$(H_2O)_{28}H^+$		
523	$(H_2O)_{29}H^+$		
541	$(H_2O)_{30}H^+$		
559	$(H_2O)_{31}H^+$		
577	$(H_2O)_{32}H^+$		
595	$(H_2O)_{33}H^+$		
613	$(H_2O)_{34}H^+$		
631	$(H_2O)_{35}H^+$		
649	$(H_2O)_{36}H^+$		
667	$(H_2O)_{37}H^+$		

685	$(H_2O)_{38}H^+$
703	$(H_2O)_{39}H^+$
721	$(H_2O)_{40}H^+$
739	$(H_2O)_{41}H^+$
757	$(H_2O)_{42}H^+$
775	$(H_2O)_{43}H^+$
793	$(H_2O)_{44}H^+$

All water cluster peaks up to m/z 800 in the positive mode were observed and shown in Table S4.

Table S5b. Water cluster peaks in the negative mode.

m/z	formula	notes	ref
17	OH⁻	[water cluster-H]⁻	[17, 18, 20]
35	H_2OOH^-		
53	$(H_2O)_2OH^-$		
71	$(H_2O)_3OH^-$		
89	$(H_2O)_4OH^-$		
107	$(H_2O)_5OH^-$		
125	$(H_2O)_6OH^-$		
143	$(H_2O)_7OH^-$		
161	$(H_2O)_8OH^-$		
179	$(H_2O)_9OH^-$		
197	$(H_2O)_{10}OH^-$		
215	$(H_2O)_{11}OH^-$		
233	$(H_2O)_{12}OH^-$		
251	$(H_2O)_{13}OH^-$		
269	$(H_2O)_{14}OH^-$		
287	$(H_2O)_{15}OH^-$		
305	$(H_2O)_{16}OH^-$		
323	$(H_2O)_{17}OH^-$		
341	$(H_2O)_{18}OH^-$		
359	$(H_2O)_{19}OH^-$		
377	$(H_2O)_{20}OH^-$		
395	$(H_2O)_{21}OH^-$		
413	$(H_2O)_{22}OH^-$		
431	$(H_2O)_{23}OH^-$		
449	$(H_2O)_{24}OH^-$		
467	$(H_2O)_{25}OH^-$		
485	$(H_2O)_{26}OH^-$		
503	$(H_2O)_{27}OH^-$		
521	$(H_2O)_{28}OH^-$		
539	$(H_2O)_{29}OH^-$		
557	$(H_2O)_{30}OH^-$		
575	$(H_2O)_{31}OH^-$		
593	$(H_2O)_{32}OH^-$		
611	$(H_2O)_{33}OH^-$		
629	$(H_2O)_{34}OH^-$		
647	$(H_2O)_{35}OH^-$		
665	$(H_2O)_{36}OH^-$		

683	$(H_2O)_{37}OH^-$
701	$(H_2O)_{38}OH^-$
719	$(H_2O)_{39}OH^-$
737	$(H_2O)_{40}OH^-$
755	$(H_2O)_{41}OH^-$
773	$(H_2O)_{42}OH^-$
791	$(H_2O)_{43}OH^-$

All water cluster peaks up to m/z 800 in the negative mode were observed and shown in Table S6.

Table S6a. Interference peaks removed in all peak PCA analysis in the positive mode.

m/z	formula	notes	ref
1	H^+	molecular fragments	[9]
12	C^+	molecular fragments	[9]
13	CH^+	molecular fragments	[9]
14	CH_2^+	molecular fragments	[9]
15	CH_3^+	molecular fragments	[9]
27	$C_2H_3^+$	molecular fragments	[10]
28	Si^+	Si wafer interference	[9]
29	$C_2H_5^+$	molecular fragments	[9]
30	SiH_2^+	Si wafer interference	[9]
41	$C_3H_5^+$	molecular fragments	[9]
45	$SiHO^+$	Si wafer interference	[9]
73	$SiC_3H_9^+$	PDMS interference	[10]
133	$Si_2C_4H_{13}O^+$	PDMS interference	[10]
147	$Si_2C_5H_{15}O^+$	PDMS interference	[10]
207	$Si_3C_5H_{15}O_3^+$	PDMS interference	[10]
209	Bi^+	Bi^+	[11]
211	$C_{13}N_3H_{13}^+$	$(M-H)^+$	[12]
212	$C_{13}N_3H_{14}^+$	diphenyl guanidine in DI water(M)	[12]
213	$C_{13}N_3H_{15}^+$	$(M+H)^+$	[12]
418	Bi_2^+	Bi_2^+	[11]
627	Bi_3^+	Bi_3^+	[11]

Interference peaks were removed in the all peak PCA analysis.

Table S6b. Interference peaks removed in all peak PCA analysis in the negative mode.

m/z	formula	notes	ref
1	H^-	molecular fragments	[9]
12	C^-	molecular fragments	[9]
13	CH^-	molecular fragments	[5]
14	CH_2^-	molecular fragments	[9]
15	CH_3^-	molecular fragments	[9]
16	O^-	molecular fragments	[13]
17	OH^-	molecular fragments	[13]
25	C_2H^-	molecular fragments	[9]
26	CN^-	molecular fragments	[5]
27	$C_2H_3^-$	molecular fragments	[9]
28	Si^-	Si wafer interference	[9]
29	SiH^-	Si wafer interference	[9]
30	SiH_2^-	Si wafer interference	[9]
49	C_4H^-	molecular fragments	[5]
60	SiO_2^-	Si wafer interference	[9]
61	$SiHO_2^-$	Si wafer interference	[9]
137	$(SiO_2)_2 OH^-$	PDMS interference	[10]
197	$(SiO_2)_3 OH^-$	PDMS interference	[10]

All peak spectralPCA analyses were done after removing the above interference peaks.

Supporting Information

List of movies

Movies of 3D images are provided to facilitate visualization of the key products. These components correspond to the 3D images in Figures 6a and 6b. Twomovies (positive mode and negative mode) are provided from 4 hr. UV and 5 hr. dark samples as the following:

In the positive ion mode, 3D movies consisting of 1. Small water clusters m/z^+ 55, 109, 199; 2. Large water clusters m/z^+ 397, 559, 631; 3. Hydrated products m/z^+ 59, 77, 79; 4. Oligomers m/z^+ 327, 461, 521; 5.Carboxylic acid m/z^+ 75, 105, 119; 6.Cluster ions and oligomers m/z^+ 193, 317, 435; respectively.

Similarly, in the negative ion mode, 3D movies consisting of 1. Small water clusters m/z^- 71, 125, 179; 2. Large water clustersm/z^- 341, 431, 557; 3. Carboxylic acid and hydration products m/z^- 59, 77, 91; 4.Oligomers m/z^- 422, 617, 635; 5.Carboxylic acid 1 m/z^- 45, 73, 89; 6.Carboxylic acid 2 m/z^+ 103, 133, 149; 7.Cluster ions m/z^- 165, 241, 329; respectively.

The color legend is listed in Tables S6a and S6b for convenience of viewing.

Table S7a. List of the positive m/z peaks in the 3D movie.

species	m/z	formula	notes	color legend
small water cluster	55	$(H_2O)_3H^+$	water cluster	I
	109	$(H_2O)_6H^+$	water cluster	I
	199	$(H_2O)_{11}H^+$	water cluster	I
large water cluster	397	$(H_2O)_{22}H^+$	water cluster	I
	559	$(H_2O)_{31}H^+$	water cluster	I
	631	$(H_2O)_{35}H^+$	water cluster	I
hydrated products	59	$C_2H_3O_2^+$	glyoxal molecular	I
	77	$C_2H_5O_3^+$	glycolic acid	I
	79	$C_2H_7O_3^+$	hydrated glycolaldehyde	I
oligomers	327	$C_{10}H_{15}O_{12}^+$	oligomers	I
	461	$C_{14}H_{21}O_{17}^+$	oligomers	I
	521	$C_{18}H_{17}O_{18}^+$	oligomers	I
carboxylic acid	75	$C_2H_3O_3^+$	glyoxylic acid	I
	105	$C_3H_5O_4^+$	malonic acid	I
	119	$C_4H_7O_4^+$	succinic acid	I
oligomers and cluster ions	193	$C_7H_{13}O_6^+$	oligomers	I
	317	$C_9H_{17}O_{12}^+$	cluster ions	I
	435	$C_{13}H_{23}O_{16}^+$	oligomers	I

Table S7b. List of the negative m/z peaks in the 3D movie.

species	m/z	formula	notes	color legend
small water cluster	71	$(H_2O)_3OH^-$	water cluster	I
	125	$(H_2O)_6OH^-$	water cluster	I
	179	$(H_2O)_9OH^-$	water cluster	I
large water cluster	341	$(H_2O)_{18}OH^-$	water cluster	I
	431	$(H_2O)_{23}OH^-$	water cluster	I
	557	$(H_2O)_{30}OH^-$	water cluster	I
hydrated and oxidation products	59	$C_2H_3O_2^-$	acetic acid	I
	77	$C_2H_5O_3^-$	gycolaldehyde dimer	I
	91	$C_2H_3O_4^-$	hydrated form of glyoxalic acid	I
oligomers	422	$C_{10}H_{15}O_{12}^-$	oligomers	I
	617	$C_{14}H_{21}O_{17}^-$	oligomers	I
	635	$C_{18}H_{17}O_{18}^-$	oligomers	I
carboxylic acid 1	45	CHO_2^-	formic acid	I
	73	$C_2HO_3^-$	glyoxylic acid	I
	89	$C_2HO_4^-$	oxalic acid	I
carboxylic acid 2	103	$C_3H_3O_4^-$	malonic acid	I
	133	$C_4H_5O_5^-$	malic acid	I
	149	$C_4H_5O_6^-$	tartaric acid	I
cluster ions	165	$C_4H_5O_7^-$	cluster ions	I
	241	$C_6H_9O_{10}^-$	cluster ions	I
	329	$C_9H_{13}O_{13}^-$	cluster ions	I

Supporting Information

Reference

1. A. G. Carlton, B. J. Turpin, K. E. Altieri, S. Seitzinger, A. Reff, H.-J. Lim and B. Ervens, *Atoms. Environ.*, 2007, **41**, 7588-7602.
2. L. Yang, X. Y. Yu, Z. H. Zhu, T. Thevuthasan and J. P. Cowin, *J. Vac. Sci. Technol. A*, 2011, **29**.
3. L. Yang, X. Y. Yu, Z. H. Zhu, M. J. Iedema and J. P. Cowin, *Lab. Chip.*, 2011, **11**, 2481-2484.
4. F. M. Green, I. S. Gilmore and M. P. Seah, *J. Am. Soc. Mass Spectrom.*, 2006, **17**, 514-523.
5. X. Hua, M. J. Marshall, Y. J. Xiong, X. Ma, Y. F. Zhou, A. E. Tucker, Z. H. Zhu, S. Q. Liu and X. Y. Yu, *Biomicrofluidics*, 2015, **9**.
6. V. F. McNeill, *Environ. Sci. Technol.* , 2015, **49**, 1237-1244.
7. X. Hua, C. Szymanski, Z. Wang, Y. Zhou, X. Ma, J. Yu, J. Evans, G. Orr, S. Liu, Z. Zhu and X. Y. Yu, *Integr. Biol.* , 2016, DOI: 10.1039/c5ib00308c.
8. X. Hua, X. Y. Yu, Z. Y. Wang, L. Yang, B. W. Liu, Z. H. Zhu, A. E. Tucker, W. B. Chrisler, E. A. Hill, T. Thevuthasan, Y. H. Lin, S. Q. Liu and M. J. Marshall, *Analyst*, 2014, **139**, 1609-1613.
9. F. Schweitzer, L. Magi, P. Mirabel and C. George, *J. Phys. Chem. A*, 1998, **102**, 593-600.
10. B. Ervens and R. Volkamer, *Atmo. Chem. Phys.* , 2010, **10**, 8219-8244.
11. A. L. Corrigan, S. W. Hanley and D. O. Haan, *Environ. Sci. Technol.* , 2008, **42**, 4428-4433.
12. Y. Tan, M. J. Perri, S. P. Seitzinger and B. J. Turpin, *Environ. Sci. Technol.*, 2009, **43**, 8105-8112.
13. E. A. Pillar, R. C. Camm and M. I. Guzman, *Environ. Sci. Technol.*, 2014, **48**, 14352-14360.
14. Y. B. Lim, Y. Tan, M. J. Perri, S. P. Seitzinger and B. J. Turpin, *Atmo. Chem. Phys.* , 2010, **10**, 10521-10539.
15. W. P. Hastings, C. A. Koehler, E. L. Bailey and D. O. De Haan, *Environ. Sci. Technol.*, 2005, **39**, 8728-8735.
16. V. Vaida, *J. Chem. Phys.*, 2011, **135**, 020901.
17. S. Jahangiri, L. M. Cai and G. H. Peslherbe, *J. Comput. Chem.*, 2014, **35**, 1707-1715.
18. R. B. Gerber, M. E. Varner, A. D. Hammerich, S. Riikonen, G. Murdachaew, D. Shemesh and B. J. Finlayson-Pitts, *Accounts Chem. Res.*, 2015, **48**, 399-406.
19. B. Ervens, B. J. Turpin and R. J. Weber, *Atmo. Chem. Phys.*, 2011, **11**, 11069-11102.
20. J. R. R. Verlet, A. E. Bragg, A. Kammrath, O. Cheshnovsky and D. M. Neumark, *Science*, 2005, **307**, 93-96.